EUROPEAN ORGANIZATION FOR NUCLEAR RESEARCH (CERN)

Measurement of the $W \to \mu\nu$ cross-sections as a function of the muon transverse momentum in pp collisions at 5.02 TeV

LHCb collaboration[†]

Abstract

The $pp \to W^{\pm}(\to \mu^{\pm}\nu_{\mu})X$ cross-sections are measured at a proton-proton centre-of-mass energy $\sqrt{s} = 5.02$ TeV using a dataset corresponding to an integrated luminosity of 100 pb^{-1} recorded by the LHCb experiment. Considering muons in the pseudorapidity range $2.2 < \eta < 4.4$, the cross-sections are measured differentially in twelve intervals of muon transverse momentum between $28 < p_{\mathrm{T}} < 52$ GeV. Integrated over p_{T}, the measured cross-sections are

$$\sigma_{W^+ \to \mu^+ \nu_\mu} = 300.9 \pm 2.4 \pm 3.8 \pm 6.0 \text{ pb},$$
$$\sigma_{W^- \to \mu^- \bar{\nu}_\mu} = 236.9 \pm 2.1 \pm 2.7 \pm 4.7 \text{ pb},$$

where the first uncertainties are statistical, the second are systematic, and the third are associated with the luminosity calibration. These integrated results are consistent with theoretical predictions.

This analysis introduces a new method to determine the W-boson mass using the measured differential cross-sections corrected for detector effects. The measurement is performed on this statistically limited dataset as a proof of principle and yields

$$m_W = 80369 \pm 130 \pm 33 \text{ MeV},$$

where the first uncertainty is experimental and the second is theoretical.

Submitted to JHEP

[†]Authors are listed at the end of this paper.

1 Introduction

Massive electroweak vector-boson production is one of the most precisely studied processes in proton-(anti)proton collisions. Predictions of the production cross-sections are factorised into hard-process matrix elements and parton distribution functions (PDFs), which describe the momentum distributions of the proton's quarks and gluons. At the LHC, the LHCb detector [1, 2] fully instruments the forward pseudorapidity region $2 < \eta < 5$. Massive vector-bosons with decay products reconstructed in the LHCb acceptance are boosted along the colliding beam axis, corresponding to a large rapidity. Measurements of the corresponding cross-sections can therefore constrain the PDFs at both high and low parton momentum fractions, complementing the measurements from other collider experiments. The LHCb collaboration has measured the $Z \to \mu^+\mu^-$ cross-section in proton-proton (pp) collisions at centre-of-mass energies $\sqrt{s} = 5.02$, 7, 8 and 13 TeV [3–6], and the $W \to \mu\nu$ cross-section at $\sqrt{s} = 7$ and 8 TeV [5, 7]. For a given rapidity range, measurements at smaller $\sqrt{s}$ provide constraints on the PDFs at larger momentum fractions than measurements at larger $\sqrt{s}$. The $W \to \mu\nu$ measurements are differential in muon pseudorapidity and integrated over muon transverse momenta $p_{\mathrm{T}} > 20\,\mathrm{GeV}$.[1]

The production of W bosons with decays to electron or muon final states is the basis of the most precise determinations of the W-boson mass m_W by the LEP [8] experiments, the CMS [9], ATLAS [10] and LHCb [11] experiments at the LHC, and the CDF [12] and D0 [13] experiments at the Fermilab Tevatron. The LHC analyses are based primarily on the charged-lepton p_{T} distribution, while the transverse mass distribution provided the strongest sensitivity in the Tevatron analyses. All of these measurements are based on fits to the observed number of W candidates, in which the model accounts for the detector resolution and efficiency, the background contamination, and the physics of the signal process. A drawback of this approach, which has been highlighted by a recent effort [14] to reconcile the results from CDF [12], LEP [8] and other experiments, is that the theoretical modelling of the signal process is deeply embedded in the analyses. This compromises the responsiveness to theoretical developments and the engagement of the theoretical community in the analyses. Ideally, the problem would be factorised into differential cross-section measurements and subsequent m_W fits, which can be reproduced, independently scrutinised, and repeated as the theoretical models evolve.

Previous LHCb W-boson cross-section analyses could not be differential in the muon p_{T} because the shape of the p_{T} distribution was the basis of the hadronic background subtraction. This paper presents a new measurement of the differential cross-section $\mathrm{d}\sigma_{W \to \mu\nu}/\mathrm{d}p_{\mathrm{T}}$, following similar measurements by CMS [15] and ATLAS [16] experiments. For the first time, the cross-section is measured differentially and used in a subsequent determination of m_W within a single analysis. The $\mathrm{d}\sigma/\mathrm{d}p_{\mathrm{T}}$ measurement is based on a fit, with simulated signal and background templates, to the number of observed signal candidates in intervals of muon p_{T} and muon isolation, which tends to have larger values for hadronic backgrounds than for the signal. The isolation is defined as the scalar sum of the transverse momenta of all other charged particles and electromagnetic calorimeter clusters within an angular separation $(\Delta\eta)^2 + (\Delta\phi)^2 < 0.5^2$, where ϕ denotes the azimuthal angle. This definition implies that a well-isolated particle has a small isolation value. The fit simultaneously corrects the data for backgrounds and the detector resolution and efficiency.

---

[1]Natural units with $\hbar = c = 1$ are used throughout.

No assumption is made on the shape of the p_T distribution of the signal.

This analysis uses a dataset of pp collisions at $\sqrt{s} = 5.02\,\text{TeV}$, recorded during a two-week period in 2017, and corresponding to an integrated luminosity of $\mathcal{L}_{\text{int}} = 100 \pm 2\,\text{pb}^{-1}$ [17], acting as a proof-of-principle to measure m_W using this novel approach. The differential cross-section is measured in the fiducial region defined by $2.2 < \eta < 4.4$, in twelve intervals of transverse momentum spaced equally in the range $28 < p_T < 52\,\text{GeV}$. In this paper, Sec. 2 describes the LHCb detector, the dataset used for this study, and the selection of signal candidates. Section 3 details corrections applied to the simulated samples, while Sec. 4 describes the hadronic background modelling. Section 5 describes the differential cross-section measurement method and results, while Sec. 6 compares the integrated results with predictions. In Sec. 7, the proof-of-principle m_W determination is presented, while Sec. 8 presents a series of cross-checks, before Sec. 9 concludes this paper.

2 Detector description and event selection

The LHCb detector used to collect the data for this analysis is described in detail in Refs. [1, 2]. The subdetector systems most relevant for this measurement include a high-precision tracking system consisting of a silicon-strip vertex detector surrounding the pp interaction region [18], a large-area silicon-strip detector (the TT) located upstream of a dipole magnet with a bending power of about $4\,\text{T m}$, and three stations of silicon-strip detectors and straw drift tubes [19] placed downstream of the magnet. The tracking system provides a measurement of the momentum p of charged particles with a relative uncertainty of around 1% at $p \approx 200\,\text{GeV}$ [2]. Photons, electrons and hadrons are identified by a calorimeter system consisting of scintillating-pad and preshower detectors, an electromagnetic and a hadronic calorimeter. Muons are identified by a system composed of alternating layers of iron and multiwire proportional chambers [20]. The online event selection is performed by a trigger [21], which consists of a hardware stage, based on information from the calorimeter and muon systems, followed by a software stage, which applies a full event reconstruction.

Simulation is required to model and correct for background contributions and the detector response in the $d\sigma/dp_T$ measurement. In the simulation, pp collisions are generated using PYTHIA8 [22] with a specific LHCb configuration [23]. Decays of heavy particles such as W bosons, Z bosons, and top quarks are modelled with PYTHIA8, which also models final-state photon radiation. For lighter particles, their decays are described by EVTGEN [24], in which final-state radiation is generated using PHOTOS [25]. A hadronic background simulation sample is produced using the hard-QCD processes in PYTHIA8 with a minimum transverse momentum of $18\,\text{GeV}$. The interaction of the generated particles with the detector and its response are implemented using the GEANT4 toolkit [26] as described in Ref. [27].

This analysis uses events selected by the hardware trigger requiring a muon with $p_T > 5\,\text{GeV}$. No attempt is made to reconstruct the neutrino from an imbalance of transverse momentum in the detector, while all identified muons with $p_T > 28\,\text{GeV}$ and $2.2 < \eta < 4.4$ are considered as $W \to \mu\nu$ signal candidates. The η region is slightly restricted compared to the detector coverage, as in Ref. [11], to ensure that the isolation is well measured. The background from $Z \to \mu^+\mu^-$ decays is suppressed by roughly a factor

of two, with a negligible inefficiency for the signal, by rejecting events in which there is a second muon with $p_T > 25$ GeV and $2.0 < \eta < 4.5$. Candidates must have a reasonable probability of originating from a primary pp interaction vertex, as reconstructed by the vertex detector, which suppresses the heavy-flavour hadron background. A requirement on the track-fit $\chi^2/$ndf suppresses the background from muonic decays of light long-lived hadrons. To qualify as signal candidates, the isolation value must be under 8 GeV. This criterion helps mitigate the background from hadrons, whose isolation values are around $\mathcal{O}(10\,\text{GeV})$, whereas muons originating from W- and Z-boson decays generally have $\mathcal{O}(1\,\text{GeV})$ isolation values.

Candidate $Z \to \mu^+\mu^-$ decays, reconstructed from oppositely charged muons, are used in several calibrations. They must have a dimuon mass between 77 and 105 GeV, and the muons must satisfy $p_T > 20$ GeV and $1.7 < \eta < 4.4$, in addition to the same track-fit $\chi^2/$ndf requirement imposed on the signal candidates. The minimum allowed η value is smaller than the value of 2.2 used in the selection of W-boson signal candidates. This choice increases the number of muons from Z-boson decays with $\eta > 2.2$ that are used for calibrations. Looser requirements are also imposed on the isolation and the compatibility of the tracks with a primary pp interaction vertex.

Muons from W- and Z-boson decays tend to have higher momenta than charged particles from heavy-flavour hadron decays. Thus, they are more susceptible to charge (q) dependent curvature biases, of the form $q/p \to q/p + \delta$, caused by residual misalignment effects. Furthermore, the 5.02 TeV data sample used in this analysis was recorded for only one polarity of the dipole magnet, which makes this analysis susceptible to residual curvature biases. The pseudomass method [28, 29] is used to determine the curvature bias corrections to be applied to the muons in the data. In this method, estimates of the dimuon mass in $Z \to \mu^+\mu^-$ decays are made using only the momentum of muons of a given charge, allowing charge-dependent biases to be probed. The asymmetry in the peak positions of the distributions for the two charges can be translated into estimates of the δ biases. In Ref. [29], the application of this method to the full LHCb Run-2 dataset is described, where biases of up to $\mathcal{O}(0.1\,\text{TeV}^{-1})$ are seen in the data while the simulation only exhibits very small asymmetries associated to the mixture of vector and axial-vector couplings in the $Z \to \mu^+\mu^-$ process. Applying this method to the 5.02 TeV sample, Fig. 1 shows, in intervals of muon η and ϕ, the biases in data, having also subtracted the small biases observed in the simulation. Applying these as curvature corrections to the muons in data results in an improvement of $\mathcal{O}(10\%)$ in the $Z \to \mu^+\mu^-$ mass resolution and greatly reduces the required size and complexity of the simulation corrections described in the following section.

Following the curvature bias corrections and the selections described above, 27 586 $W^+ \to \mu^+\nu_\mu$ candidates and 21 678 $W^- \to \mu^-\overline{\nu}_\mu$ candidates are retained for the d$\sigma/$dp_T measurement, and 3495 $Z \to \mu^+\mu^-$ candidates are retained for data-driven adjustments to the simulation that are described in the following section.

3 Corrections to the simulation

The simulation is used to model the muon detection efficiency and backgrounds, and subsequently to correct the data for these contributions. Corrections to the simulation are required to improve the accuracy of this model in describing the data.
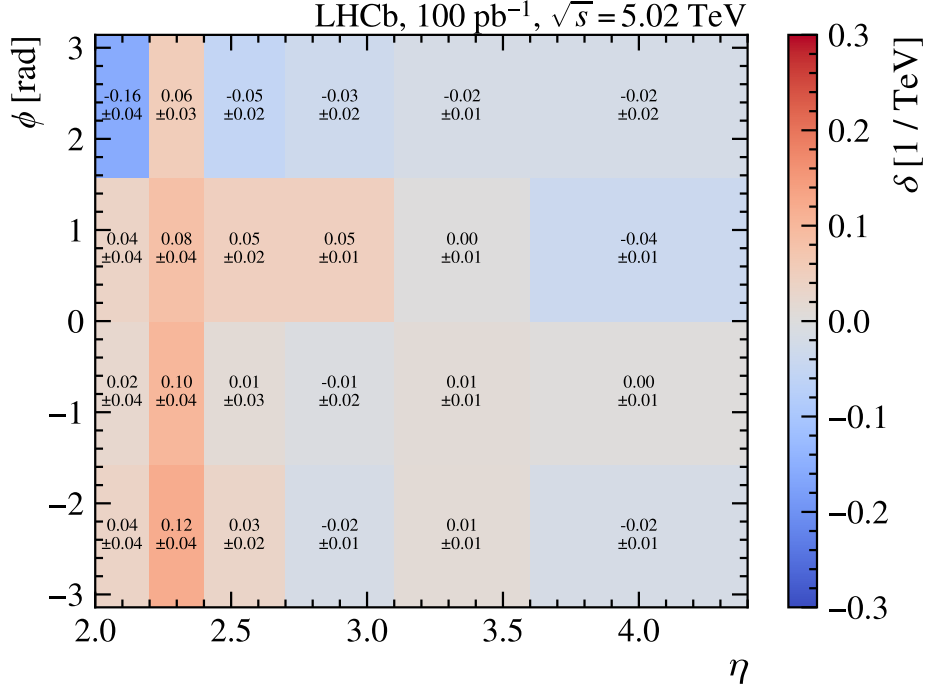
Figure 1: Biases in q/p estimated with the pseudomass method in (η, ϕ) intervals.

3.1 Muon momentum smearing

Although the pseudomass corrections improve the momentum resolution in data, some effects contributing to the momentum resolution are still underestimated in the simulation. Therefore, a smearing of the muon momenta in the simulation is required. In the simulation, the muon momenta are multiplied by a factor

$$(1 + \alpha)(1 + f_1(\eta)\mathcal{R}_1\sigma_1)(1 + pf_2(\eta)\mathcal{R}_2\sigma_2), \tag{1}$$

where $\mathcal{R}_{1,2}$ are independent random numbers sampled from a standard normal distribution, α is a momentum scale offset, and σ_1 and σ_2 are momentum and curvature smearing parameters, respectively. The function $f_1(\eta)$ is defined to be 1.0 for $\eta < 3.3$ and 1.5 for $\eta \geq 3.3$, while $f_2(\eta) = 1/\cosh\eta$.

The values for the α and σ_2 parameters are obtained by minimising the χ^2 between the $Z \to \mu^+\mu^-$ mass distribution in data and that in the simulation, where the simulation is smeared according to these parameters. Independent parameters are used for muons in the regions $\eta < 2.2$ and $2.2 < \eta < 4.4$. The $Z \to \mu^+\mu^-$ candidates are categorised as having zero, one or two muons in the $2.2 < \eta < 4.4$ region, which yields three separate dimuon mass distributions. The background is approximately three orders of magnitude smaller than the signal and can be safely neglected in the fit. The value of σ_1, which has minimal influence in this analysis, is fixed at 2×10^{-3}, similar to what was chosen for the previous m_W analysis at LHCb [11]. The χ^2 of the fit is 121.3 for 146 degrees of freedom, and the best-fit values of the other parameters are presented in Table 1. Figure 2 shows the mass distribution in data, compared to the simulation before and after the smearing with the best-fit values of the smearing parameters. While the momentum smearing only has a modest effect on the modelling of the $Z \to \mu^+\mu^-$ mass distribution in this small

4

Table 1: Results of the momentum smearing fit.

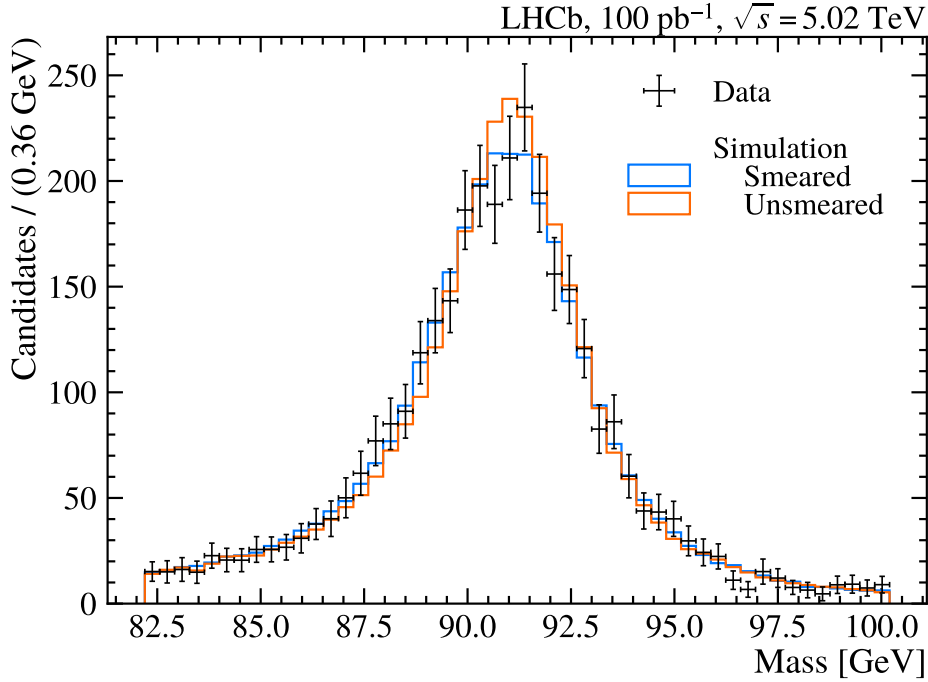| Parameter	η range	Fit result
α	$\eta < 2.2$	$(\ \ 0.2 \pm 0.9) \times 10^{-3}$
	$2.2 < \eta < 4.4$	$(-1.2 \pm 0.6) \times 10^{-3}$
σ_2	$\eta < 2.2$	$(\ 15.4 \pm 3.1) \times 10^{-5}\ \mathrm{GeV}^{-1}$
	$2.2 < \eta < 4.4$	$(\ 24.7 \pm 2.8) \times 10^{-5}\ \mathrm{GeV}^{-1}$

Figure 2: Mass distribution of the $Z \to \mu^+\mu^-$ candidates. The simulation before and after the application of the momentum smearing is also shown.

dataset, it is important to estimate and propagate the statistical uncertainties on the smearing parameters.

3.2 Muon detection efficiency

Following the approach of Ref. [11], the muon trigger, tracking, and identification efficiencies are measured from the $Z \to \mu^+\mu^-$ samples in both the data and simulation. One muon, denoted as the "tag", must satisfy the requirements of all stages of the trigger system. The fraction of candidates in which the other muon, the "probe", also satisfies the trigger requirements provides an estimate of the per-muon trigger efficiency. Similarly, a dedicated sample, without a muon-identification requirement applied to the probe, is used to estimate the corresponding efficiency. The track-reconstruction efficiency is estimated with a sample in which the probe muon is reconstructed only using hits in the muon system and the TT chambers.[2]

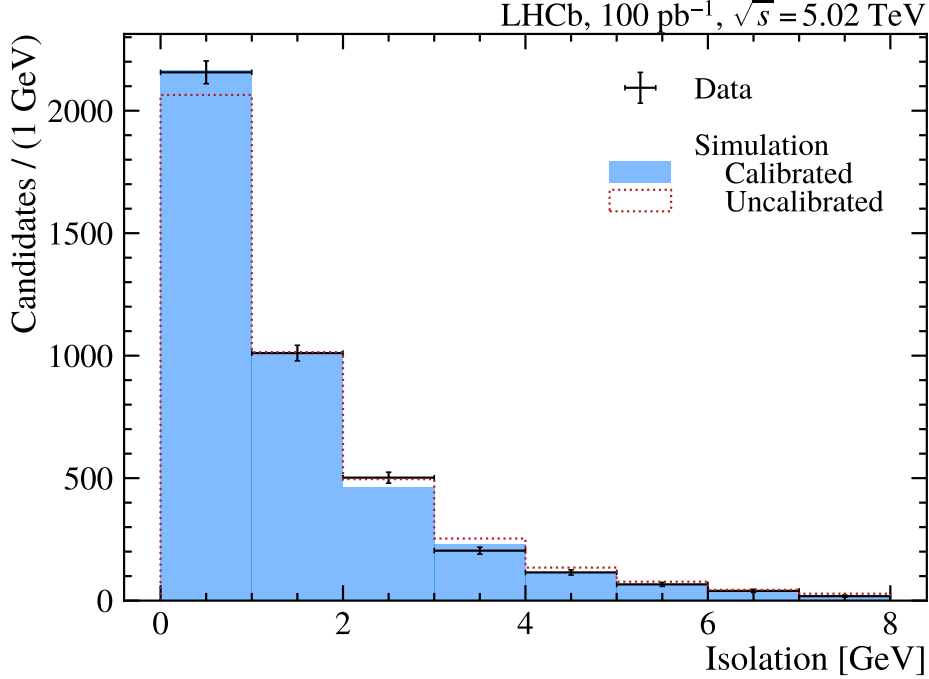[2]The standard charged-particle reconstruction does not explicitly require TT clusters.

Figure 3: Muon-isolation distribution of the $Z \to \mu^+ \mu^-$ candidates. The simulation before and after the application of the isolation calibration is also shown.

The muon trigger, tracking and identification efficiencies are estimated in five intervals of η in both data and simulation. Weights are then evaluated as the ratios of data to simulation, and used to correct for the differences in the simulated efficiencies. Identification and tracking efficiency corrections are typically within $\mathcal{O}(1\%)$ of unity for all η intervals. The trigger efficiency corrections are similarly small at low η but in the highest η interval, with $3.85 < \eta < 4.40$, the correction factor is around 0.85.

3.3 Muon-isolation calibration

Figure 3 shows the isolation variable distribution for the $Z \to \mu^+ \mu^-$ sample, including muons of both charges, compared to the simulation. The modelling of this distribution depends on both the detector response and the physics processes, including the hadronic recoil in the hard process and the underlying event. To account for inaccuracies in the simulation, a multiplicative calibration factor of 0.93 ± 0.02 is determined by fitting the simulated isolation distribution to that observed in $Z \to \mu^+ \mu^-$ data, as shown in Fig. 3. The fit yields a minimum χ^2/ndf of 16.3/13. This calibration factor is then applied to the isolation values of muons in the $W \to \mu\nu$ signal simulation.

4 Hadronic-background modelling

One of the largest sources of background among the $W \to \mu\nu$ candidates consists of light charged hadrons, which are misidentified as muons due to decays in flight or particles in hadronic showers that are not fully absorbed before the muon system. The majority of
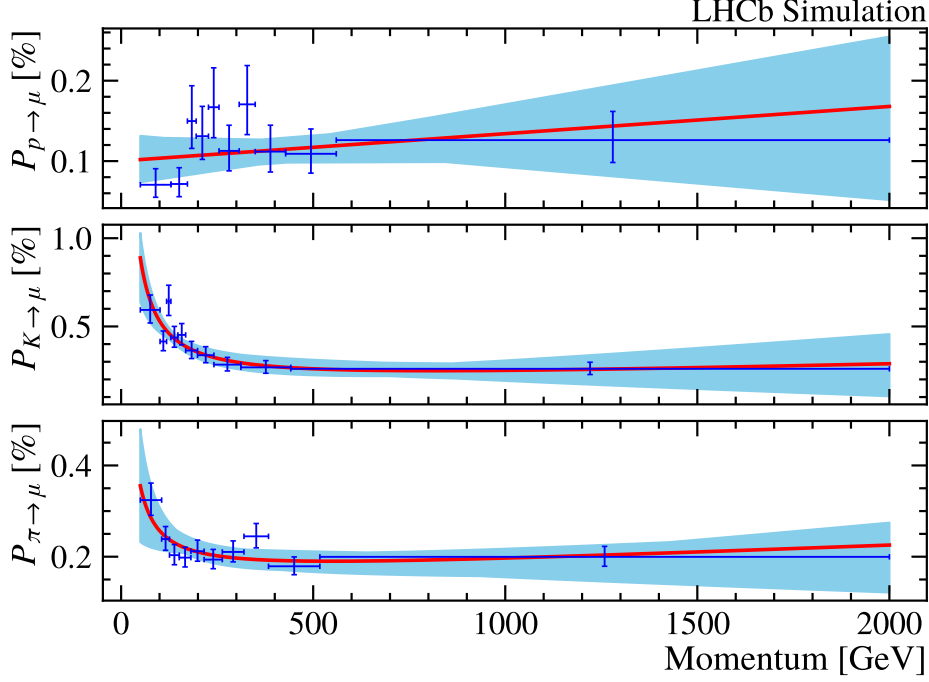
Figure 4: Momentum-dependent probabilities for (lower) pion, (central) kaon and (upper) proton misidentification as muons in the simulation. The fit results are also shown and are represented by the red lines. The blue bands show the area covered by the systematic uncertainties. Note that the misidentification probabilities correspond to the muon-identification requirements used in this analysis, which are not optimised for low momentum.

the hadronic background is where the muon candidate is actually a charged pion or kaon, with a smaller contribution coming from protons.

Figure 4 shows the probabilities for pions, kaons and protons to be misidentified as muons in the hadronic-background simulation sample. For the pions and kaons, the momentum dependence is parametrised as the sum of two components. The first accounts for decays to muons and has the form $1 + \exp\left(-ml/p\tau\right)$ for a particle of mass m and lifetime τ, where $l = 15\,\mathrm{m}$ is the approximate length of the detector up to the second muon station. The second, which increases linearly with momentum, accounts for hadronic shower particles penetrating through the calorimeters or for decays of nearby hadronic particles to muons. For protons, only the second term is included. The results of the fits of these functions to the simulated probabilities are shown in Fig. 4. The χ^2/ndf fit values for pions, kaons, and protons are 8.6/7, 8.7/7, and 13.0/8, respectively. For pions and kaons, the probabilities vary between $\mathcal{O}(10^{-3})$ and $\mathcal{O}(10^{-2})$, while for protons they are $\mathcal{O}(10^{-3})$. The parametrisations of the misidentification rates are used to assign weights that replace explicit muon-identification requirements in the simulation of the hadronic background.

To study high-p_T hadron behaviour in the data, a sample enriched in high-p_T hadrons is required. A sample is selected from the data recorded in pp collisions at $\sqrt{s} = 13\,\mathrm{TeV}$ in 2017. Since no dedicated hadron trigger was available during the $\sqrt{s} = 5.02\,\mathrm{TeV}$ run, the $13\,\mathrm{TeV}$ sample is used to calibrate the modelling of the hadronic background at $5.02\,\mathrm{TeV}$. In the software trigger, the hadron candidates are selected in the same way as the signal
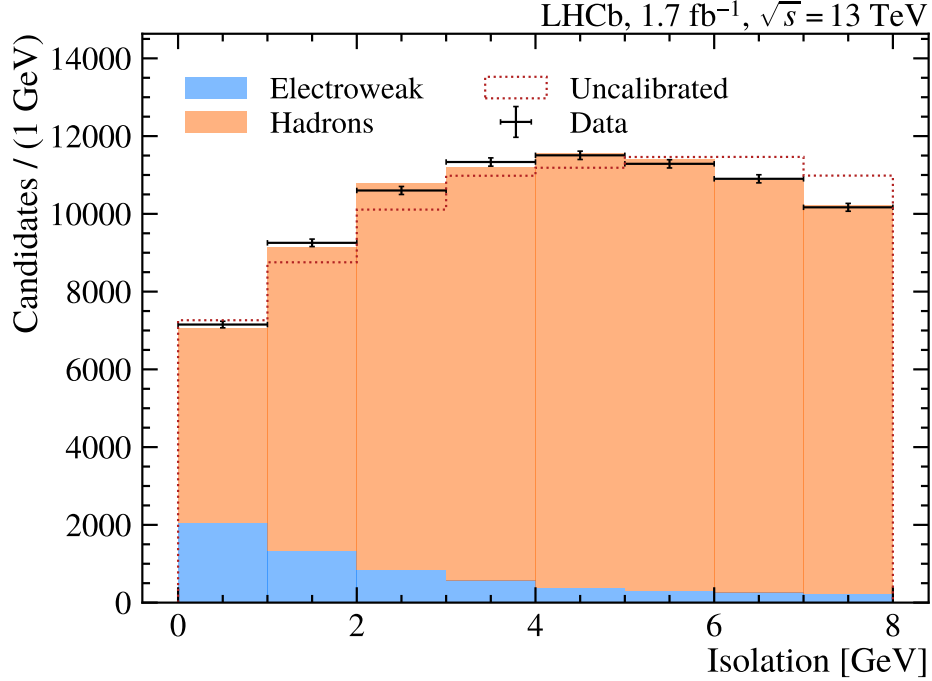
Figure 5: Muon-isolation distribution in the hadron-enriched sample, with both charges combined. The simulation before and after the application of the isolation calibration are also shown.

candidates, except that the muon-identification requirement is replaced by a randomised event selection to reduce the rate. Figure 5 shows the isolation distribution of these candidates, with the same kinematic and track-quality requirements applied as for the $W \to \mu\nu$ selection. Similarly to the muons from electroweak processes, a calibration is applied to the simulation to account for possible inaccurate modelling. A simultaneous fit is performed on the isolation distributions of the positively and negatively charged hadrons. The data are described by the sum of a small electroweak component at lower isolation values and the main hadron component, with simulation. The electroweak component is predominantly hadronic decays of τ leptons from W- and Z-boson decays. In the fit, the hadronic fraction for each charge is allowed to vary freely. The isolation values for the hadrons of charge q are scaled by a calibration factor of $f + q\zeta$, with f and ζ varying freely in the fit. The fit has a minimum χ^2/ndf of 8.2/10 and the best-fit calibration parameters are $f = 0.83 \pm 0.01$ and $\zeta = 0.05 \pm 0.01$. Figure 5 shows the distribution in data and the fit results.

5 Differential cross-section measurement

5.1 Likelihood function

The differential cross-sections $\mathrm{d}\sigma/\mathrm{d}p_\mathrm{T}$ are determined from a fit to the two-dimensional distributions of the $W \to \mu\nu$ candidates, corresponding to the product of twelve p_T intervals in the range $28 < p_\mathrm{T} < 52\,\mathrm{GeV}$ and eight intervals for the isolation below $8\,\mathrm{GeV}$. Each p_T interval has a width of $2\,\mathrm{GeV}$, which is denoted Δp_T. In data, the numbers of

candidates in the 96 intervals i of p_T and isolation are denoted k_i. The fit to these data minimises the function

$$-\ln \mathscr{L} = \sum_i^n \left[-k_i \ln \beta_i \lambda_i + \beta_i \lambda_i \right] + \frac{1}{2} \sum_{i,k}^n (\beta_i - 1) \left(\frac{C_{i,k}}{\lambda_i \lambda_k} \right)^{-1} (\beta_k - 1), \qquad (2)$$

where λ_i are the model predictions based on simulation; β_i are nuisance parameters accounting for the finite sizes of the simulation samples; and the covariance matrix C represents the total statistical uncertainty in the predictions, stemming from the limited sizes of the simulation samples. The first term in Eq. 2 represents the contribution from the Poisson probability of observing the data given the expected counts. The β values are minimised via an analytic solution [30, 31]. The model predictions are composed as

$$\lambda_i = \lambda_i^s + \lambda_i^{\text{had}} + \sum_b \lambda_i^b, \qquad (3)$$

where the first term corresponds to the signal, the second to the hadronic background, and the third to all other backgrounds.

5.2   Signal component

The signal component is predicted as

$$\lambda_i^s(d\sigma/dp_T) = \mathcal{L}_{\text{int}} \sum_j R_{ij} d\sigma/dp_{T_j} \Delta p_T, \qquad (4)$$

where R_{ij} is a response matrix, defined as

$$R_{ij} = \frac{n_{ij}^{\text{rec}} \bar{w}_{ij}}{n_j^{\text{gen}}}, \qquad (5)$$

where n_{ij}^{rec} is the number of simulated decays with a true p_T corresponding to the interval j and being reconstructed in interval i, while $\bar{w}_{ij}$ is the corresponding average efficiency weight. The denominator n_j^{gen}, which is the number of events generated with the true p_T in interval j, explicitly eliminates the dependence of this analysis on any assumption about $d\sigma/dp_T$.[3]

The response matrix has 14 intervals along the true p_T axis, where twelve of these exactly match the reconstructed p_T intervals. The other two, referred to as the "underflow" and "overflow", respectively, correspond to $26 < p_T < 28\,\text{GeV}$ and $52 < p_T < 54\,\text{GeV}$. These are effectively treated as two extra background components in the fit, but with a special treatment of their normalisations. Both cross-sections are predicted as the sum of the twelve cross-sections spanning the fiducial region, which vary freely in the fit, multiplied by factors determined from the simulation, which are fixed in the fit. With this strategy there are no freely varying parameters associated to the underflow and overflow cross-sections, and no assumption is required for their *absolute* values; only two *relative* cross-sections.

Figure 6 shows the response matrix for the W^+ decay process, having integrated over the isolation. A very similar response matrix is obtained for the W^- case. Roughly 70%

---

[3]Up to any variation in the detection efficiency within the 2 GeV intervals of p_T.
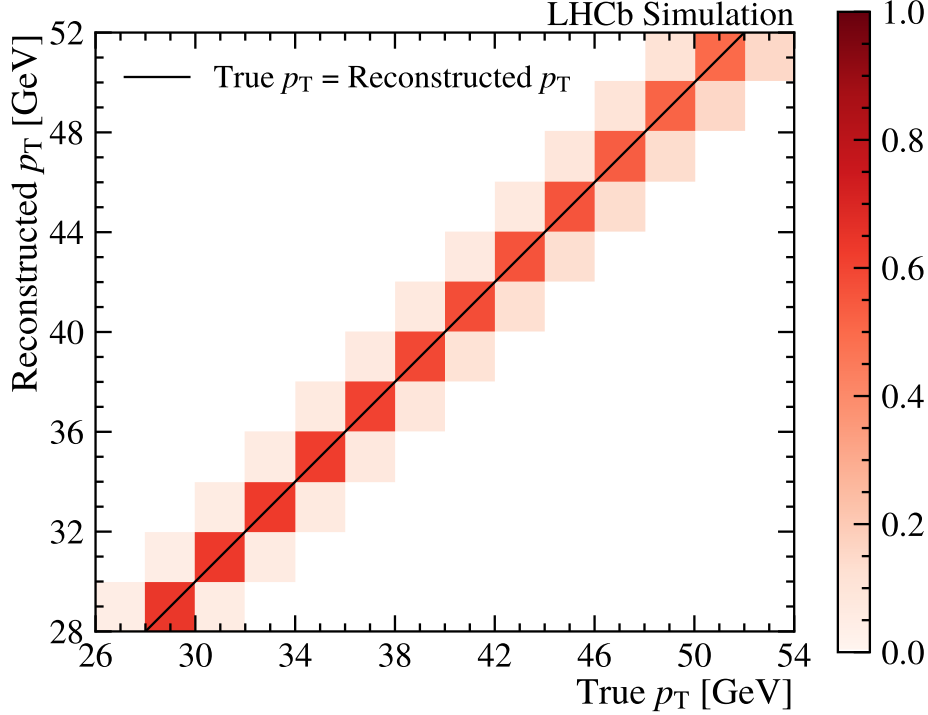
Figure 6: Response matrix for the W^+ decay, after integration over the isolation intervals.

of the signal candidates have the true and reconstructed p_{T} in the same interval, which is expected comparing the $2\,\mathrm{GeV}$ interval width with the resolution of $\mathcal{O}(1\,\mathrm{GeV})$. Statistical uncertainties and correlations from the response matrix are appropriately propagated, taking into account its multinomial nature.

5.3 Backgrounds

The light hadron background is modelled using a normalised template $t^{\mathrm{rec}}_{\mathrm{had},i}$, derived from simulation after the misidentification probability weights are applied to reconstructed hadrons. This template represents the expected shape of the background across bins, with $\sum_i t^{\mathrm{rec}}_{\mathrm{had},i} = 1$. The expected number of background events in bin i is expressed relative to the observed number of signal candidates n^{obs} as

$$\lambda^{\mathrm{had}}_i = n^{\mathrm{obs}} f_{\mathrm{had}} t^{\mathrm{rec}}_{\mathrm{had},i}, \tag{6}$$

where f_{had} is a freely varying fraction.

The remaining backgrounds from $Z \to \mu^+\mu^-$, $Z \to \tau^+\tau^-$, $W \to \tau\nu$ and decays of heavy-flavour hadrons and top quarks are modelled using simulated samples. For each background b, n^{gen}_b events are generated, resulting in a simulated distribution $n^{\mathrm{rec}}_{b,i}$. The associated fit model is

$$\lambda^b_i = \left(\frac{n^{\mathrm{obs}}_Z}{\sigma_Z \varepsilon_Z} \right) \left(\frac{n^{\mathrm{rec}}_{b,i}}{n^{\mathrm{gen}}_b} \right) \sigma_b, \tag{7}$$

where σ_b is the background process cross-section. The first factor is an estimate of the integrated luminosity based on the observed number of $Z \to \mu^+\mu^-$ events n^{obs}_Z, the

Table 2: Results of the differential cross-section fits, where the first and second uncertainties are statistical and systematic, respectively.

Interval in p_T [GeV]	$\mathrm{d}\sigma/\mathrm{d}p_\mathrm{T}$ [pb/GeV]	
	$W^+ \to \mu^+\nu_\mu$	$W^- \to \mu^-\overline{\nu}_\mu$
28–30	$11.93 \pm 0.44 \pm 0.36$	$14.81 \pm 0.47 \pm 0.35$
30–32	$14.36 \pm 0.46 \pm 0.29$	$15.70 \pm 0.48 \pm 0.26$
32–34	$17.66 \pm 0.48 \pm 0.31$	$15.59 \pm 0.48 \pm 0.24$
34–36	$18.87 \pm 0.51 \pm 0.31$	$16.09 \pm 0.48 \pm 0.29$
36–38	$22.73 \pm 0.56 \pm 0.36$	$16.53 \pm 0.49 \pm 0.24$
38–40	$23.50 \pm 0.58 \pm 0.31$	$14.57 \pm 0.48 \pm 0.32$
40–42	$17.16 \pm 0.53 \pm 0.31$	$10.26 \pm 0.42 \pm 0.24$
42–44	$10.45 \pm 0.43 \pm 0.30$	$6.13 \pm 0.35 \pm 0.18$
44–46	$6.01 \pm 0.35 \pm 0.17$	$3.28 \pm 0.28 \pm 0.23$
46–48	$3.46 \pm 0.30 \pm 0.14$	$2.41 \pm 0.24 \pm 0.14$
48–50	$2.59 \pm 0.26 \pm 0.13$	$1.65 \pm 0.22 \pm 0.15$
50–52	$1.75 \pm 0.21 \pm 0.14$	$1.42 \pm 0.18 \pm 0.11$

corresponding cross-section σ_Z and the simulated efficiency ε_Z. The cross-sections are evaluated at $\mathcal{O}(\alpha_s^2)$ using the MCFM [32] program with the NNPDF4.0 parton distribution functions.[4] The backgrounds from heavy-flavour hadron decays are included with the leading-order cross-section computed using PYTHIA8.

5.4 Fit results

Figure 7 shows the $(p_\mathrm{T}, \text{isolation})$ distributions and the fit results, which are independent for the W^+ and W^- distributions. In each case, there are 12×8 intervals, and there are 12 freely varying $\mathrm{d}\sigma/\mathrm{d}p_\mathrm{T}$ values and 1 freely varying hadronic background parameter, corresponding to 83 degrees of freedom. The fit minima correspond to χ^2 values of 131.6 and 85.4 for the $W^+ \to \mu^+\nu_\mu$ and $W^- \to \mu^-\overline{\nu}_\mu$ fits, respectively.[5] The best-fit $\mathrm{d}\sigma/\mathrm{d}p_\mathrm{T}$ values and the statistical uncertainties are presented in Table 2. Figure 8 shows the correlation matrix corresponding to the statistical uncertainties for the fit to the $W^+ \to \mu^+\nu_\mu$ data. Moving away from the diagonal, a pattern of alternating negative and positive correlations is seen but this is damped to the $\mathcal{O}(1\%)$ level after two cells away from the diagonal. The corresponding matrix for the other W-boson charge is similar.

5.5 Systematic uncertainties

The total systematic uncertainty on the differential cross-section measurement is represented by a single 24×24 covariance matrix. This corresponds to twelve p_T intervals for W^+ and W^- bosons respectively, because some sources of uncertainty are strongly correlated (or anticorrelated) between the two. A covariance matrix is defined for each source and these are added linearly, and for some sources the covariances for more than

---

[4]In this paper α_s denotes the strong coupling evaluated at a scale corresponding to the Z-boson mass.
[5]The χ^2 calculation accounts for the constant terms in the log-likelihood that are commonly omitted since they do not depend on the fit parameters.
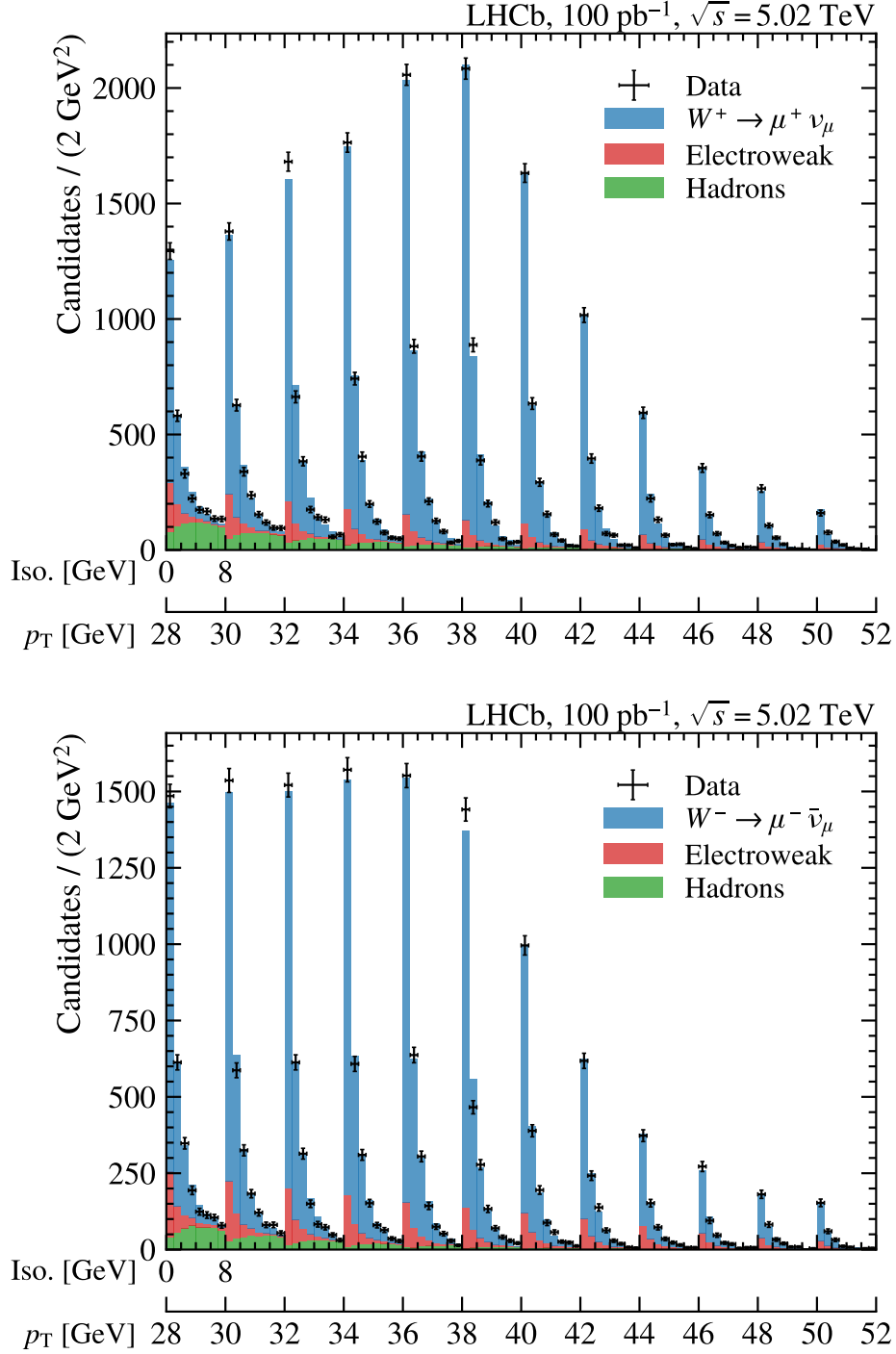
Figure 7: Distributions of p_T and isolation for the (upper) W^+ and (lower) W^- candidates. Eight intervals of isolation up to 8 GeV are repeated over the twelve p_T intervals. The results of the differential cross-section fits are also shown, where the electroweak background component includes the relatively small contribution from heavy-flavour hadron decays.
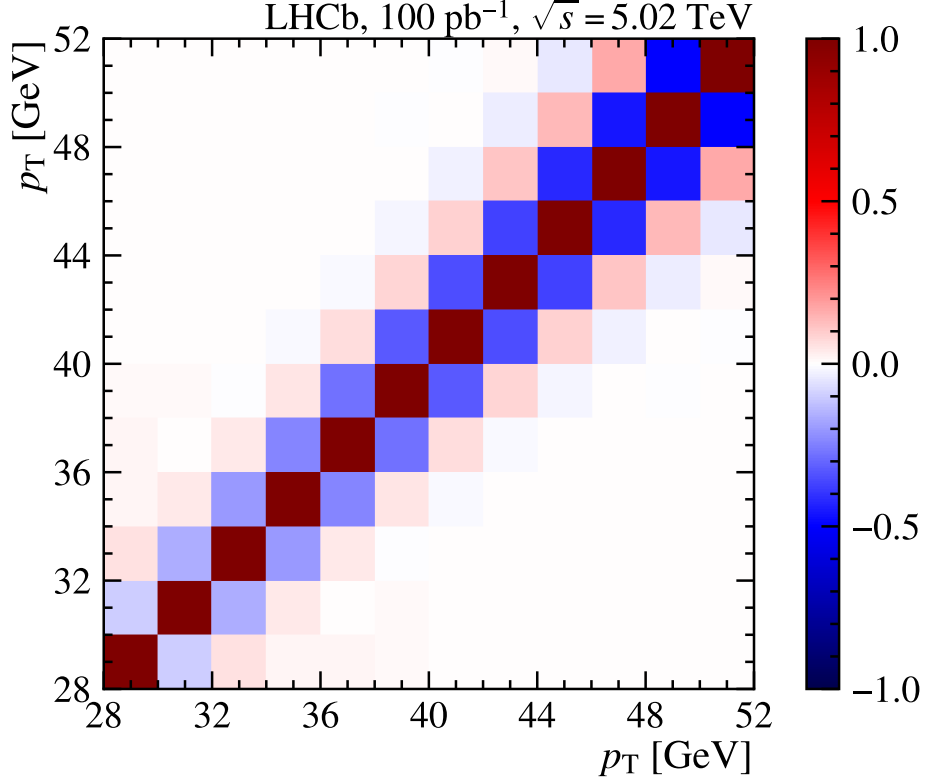
Figure 8: Correlation matrix corresponding to the statistical uncertainties on the $d\sigma/dp_T$ fit results for the W^+ process. The same qualitative patterns are seen for the equivalent figure for the other W-boson charge.

one subsource are combined. The sources of systematic uncertainty are categorised as follows.

Muon efficiency: The statistical uncertainties associated with the trigger, tracking and identification efficiency of muons are propagated to the differential cross-section fit by repeatedly varying each correction factor according to a Gaussian distribution defined by its central value and associated uncertainty, and refitting the cross-section. The effect of variations in the η binning schemes is found to be negligible compared to the other uncertainties in this analysis.

Charge-independent momentum biases: The covariance of the momentum smearing fit result is propagated through the simulation by repeating the cross-section fit with random sampling.

Charge-dependent momentum biases: The statistical uncertainties on the pseudo-mass corrections are uncorrelated between the (η, ϕ) intervals. While the corrections are applied to the data, their statistical uncertainties are propagated by applying charge-dependent curvature shifts to the muon momenta in the simulation. The shifts are sampled from normal distributions representing the corrections and their uncertainties. The differential cross-section fit is repeated several times and the standard deviation in the fit results is defined as the uncertainty.

Hadronic background: The corresponding uncertainties are fourfold. The first is the covariance from the fits of the momentum-dependent misidentification function propagated by random sampling. The second uncertainty is determined by varying the weights assigned separately to pions, kaons, and protons by a conservative $\pm 20\%$ [33]. The third uncertainty is the statistical uncertainty associated with the isolation calibration factor. The fourth uncertainty considers a different model that includes the hadronic background p_{T} shape, which is described in Eq. 8. This alternative model (weight strategy) includes one additional factor,

$$\left(1 + w\frac{p_{\mathrm{T}} - \bar{p}_{\mathrm{T}}}{N_{\mathrm{bins}}}\right),\tag{8}$$

where w modifies the shape of the p_{T} distribution, p_{T} is the bin centre in muon transverse momentum, and $\bar{p}_{\mathrm{T}}$ is the median p_{T} value (40 GeV). The default fit model corresponds to $w = 0$.

Isolation: This includes the statistical uncertainty of the isolation calibration factors and the choice of the number of isolation intervals, which is changed from eight to six or ten. The statistical uncertainty on the isolation calibration factor is also propagated by repeating the cross-section fit with this factor shifted up and down by one standard deviation.

Unfolding: This accounts for the uncertainty resulting from increasing or decreasing the counts of underflow and overflow intervals by 10%. Furthermore, the number of reconstructed p_{T} bins is varied, increasing from twelve to twenty-four while keeping twelve true p_{T} bins.

Figure 9 shows the relative uncertainty for each category. Figure 10 shows the correlation matrix corresponding to the sum of the covariance matrices for each category. The largest source of uncertainty for the W^+ boson is the charge-dependent momentum bias, which reaches around 7% in the highest p_{T} interval. However, this source is strongly anticorrelated between the W^+ and W^- bosons, which is the cause of the regions of negative correlation seen in Fig. 10. It is crucial that this anticorrelation is correctly accounted for in a fit for m_W. The largest source of uncertainty for the W^- boson is the so-called unfolding uncertainty, which peaks at around 8% at higher p_{T} intervals. This is driven by varying the number of reconstructed-level p_{T} bins from twelve to twenty-four. The next largest source of uncertainty for both charges is the muon efficiency, at a level of around 1%. This source is strongly correlated across all twenty-four p_{T} intervals.

6 Integrated cross-sections and comparison with predictions

Integrating the differential results over p_{T} gives:

$$\sigma_{W^+ \to \mu^+ \nu_\mu} = 300.9 \pm 2.4 \pm 3.8 \pm 6.0\,\mathrm{pb},$$
$$\sigma_{W^- \to \mu^- \bar{\nu}_\mu} = 236.9 \pm 2.1 \pm 2.7 \pm 4.7\,\mathrm{pb},$$

where the first uncertainty is statistical, the second is systematic, and the third comes from the integrated luminosity. The correlation between the total uncertainties in the W^+
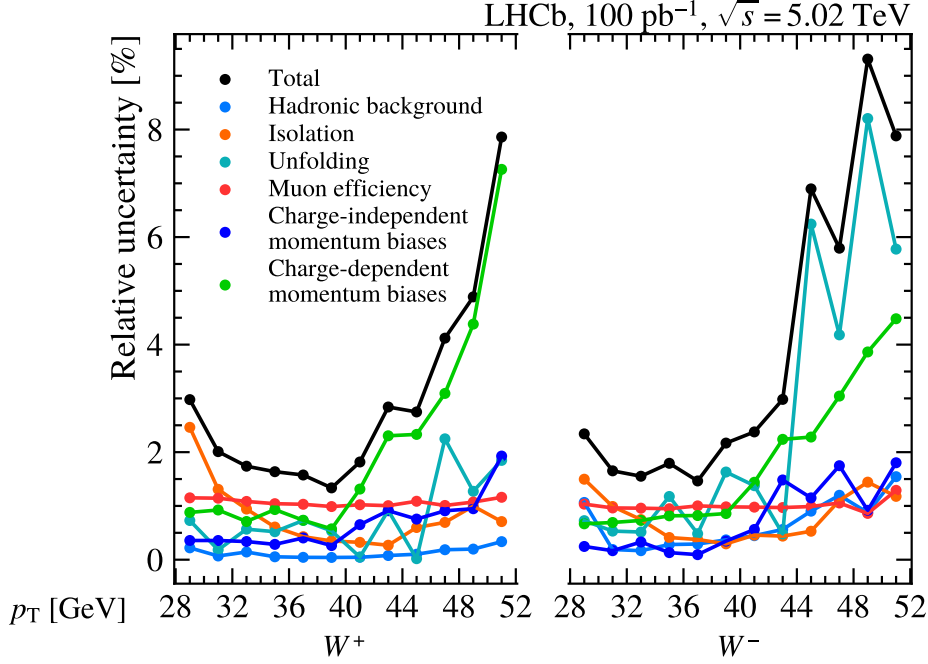
Figure 9: Relative systematic uncertainties on the (left) W^+ and (right) W^- differential cross-sections as a function of p_T. These are obtained by dividing the systematic uncertainty in each bin by the corresponding cross-section value, as listed in Table 2.

and W^- cross-sections is 0.84. Figure 11 compares these results with predictions at $\mathcal{O}(\alpha_s^2)$ from MCFM with the CT18 [34], NNPDF3.1 [35], NNPDF4.0 [36] and MSHT20 [37] PDF sets.[6] The presented predictions include uncertainties from the PDF sets and variations in the scales. The renormalisation and factorisation scales are independently multiplied by factors of 0.5 and 2 around their central values, which correspond to the W-boson mass. Of the 3×3 possible combinations, those in which the two scales vary in opposite directions are excluded. The associated uncertainty is defined as the maximum variation out of the seven remaining scale combinations [38]. The measurement is consistent with the predictions.

7 Determination of the W-boson mass

7.1 Overview of the fit model

The differential cross-section data can now be used in a fit for m_W. The fit minimises the χ^2 between the data and theoretical templates with m_W as a free parameter. The model is derived from that used in the m_W fit of Ref. [11]. The $pp \to W^\pm (\to \mu^\pm \nu_\mu) X$ events are generated using PYTHIA8 with the same version and tune as the samples with full detector simulation. As in Ref. [11], the model can mimic a variation in m_W with the use of weights from an analytic function of the true boson mass. Weights are assigned to map these samples to the average of the predictions of PYTHIA8, PHOTOS and HERWIG [39],

---
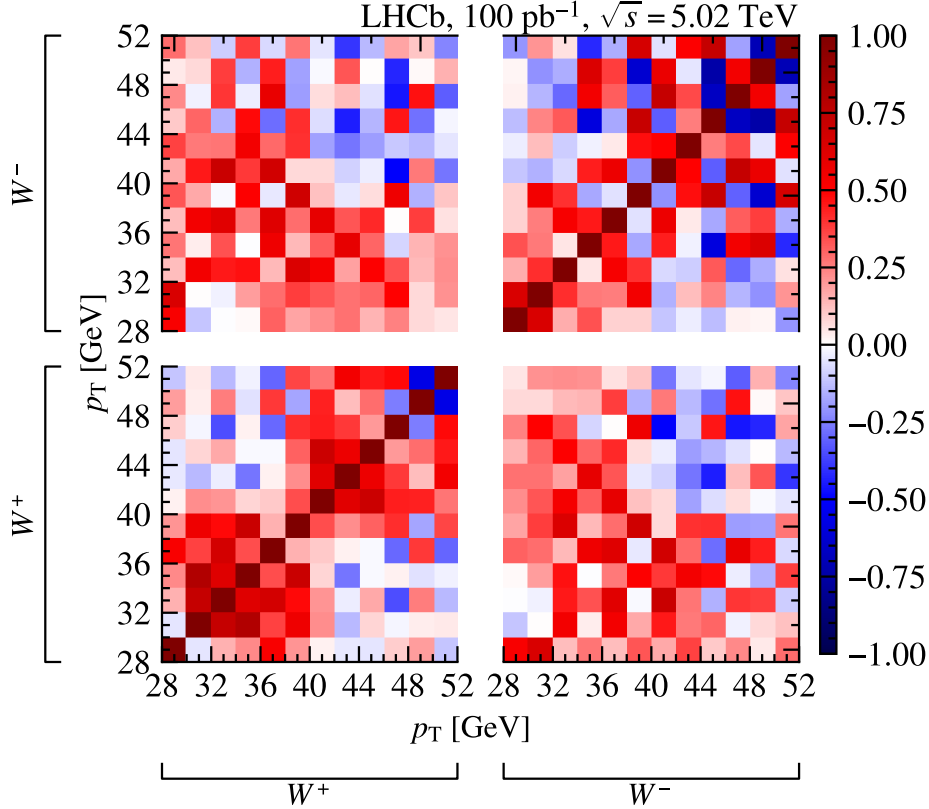
[6]These PDFs are evaluated at NNLO.

Figure 10: Correlation matrix corresponding to the total systematic uncertainty, with rows and columns ordered as W^+ and then W^-.

in the distribution of the energy difference between the dilepton system before and after final-state radiation.

Since Pythia8 only includes the leading p_T-logarithms in the perturbative series in the strong coupling α_s, through its parton shower, further corrections are required. Following the approach of Ref. [11], the differential cross-section is factorised into an unpolarised factor and a closed-form sum of angular functions with eight angular coefficients. These are differential in the dilepton rapidity and p_T.[7] The two angular degrees of freedom are defined in the Collins–Soper frame [40]. The event sample is assigned weights based on the ratio of the cross-sections of Pythia8 compared to a target prediction.

The target predictions are based on the DYTurbo [41] program. Following Refs. [11, 42], the analysis is performed with models based on the NNPDF3.1, MSHT20, and CT18 PDF sets, and the final result is a simple arithmetic average of those obtained with the three separate PDF sets. The unpolarised cross-sections are based on the summation of the large p_T-logarithms up to the second order, followed by matching to exact $\mathcal{O}(\alpha_s^2)$ calculations. The angular coefficients are calculated at $\mathcal{O}(\alpha_s)$ accuracy. For the unpolarised cross-sections, the predictions are made for a range of α_s and g values, where g encodes the nonperturbative dynamics affecting the p_T distribution of the partons.

---

[7]These also have a mass dependence, but this has a negligible effect in the present analysis.

7.2 Validation fit to Z-boson production cross-section data

Figure 12 shows the Z-boson $d\sigma/dp_T$ data at $5.02\,\mathrm{TeV}$ published by the LHCb collaboration [3]. The data are compared to the model described in the previous section, with the NNPDF3.1 PDF set and with $\alpha_s = 0.118$ and $g = 1\,\mathrm{GeV}^2$. It can be seen that the DYTURBO prediction, after normalising to the data, overestimates the cross-section in the first two bins, but is below the data in a broad region around $10\,\mathrm{GeV}$. A fit in which the normalisation, α_s and g are allowed to vary freely gives a χ^2/ndf of $10.4/8$. Furthermore, it favours an increased value of $g = 1.95 \pm 0.49\,\mathrm{GeV}^2$, which suppresses the first two bins, and a decreased value of $\alpha_s = 0.112 \pm 0.006$,[8] which improves the description at higher p_T.

7.3 Determination of the W-boson mass

Figure 13 shows the W-boson $d\sigma/dp_T$ data compared to the results of a fit, based on the NNPDF3.1 PDF set, with the α_s value fixed to that determined from the Z-boson data using the same PDF set, and the g and m_W values varying freely. This gives a χ^2/ndf of $25.6/21$, and best-fit values of $m_W = 80366 \pm 130\,\mathrm{MeV}$ and $g = 1.1 \pm 0.6\,\mathrm{GeV}^2$. This fit includes all sources of uncertainty on the $d\sigma/dp_T$ measurement, via the 24×24 covariance matrix. The following additional sources of theoretical uncertainties are assessed for the mass measurement:

Strong coupling value: The statistical uncertainty from the fit to the Z-boson data is propagated by repeating the m_W fit with this value shifted by one standard deviation in the two directions. The resulting uncertainty is $16\,\mathrm{MeV}$.
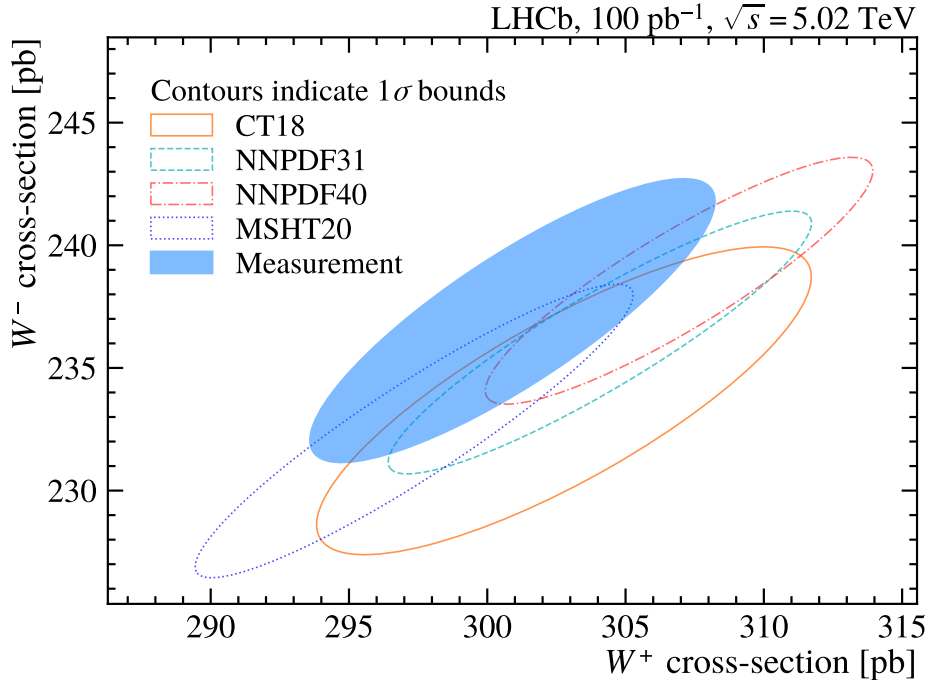

Figure 11: Integrated cross-sections compared to $\mathcal{O}(\alpha_s^2)$ predictions.

---

[8]This should not be considered as a robust determination of α_s. A full assessment of the theoretical uncertainties is beyond the scope of the present analysis.
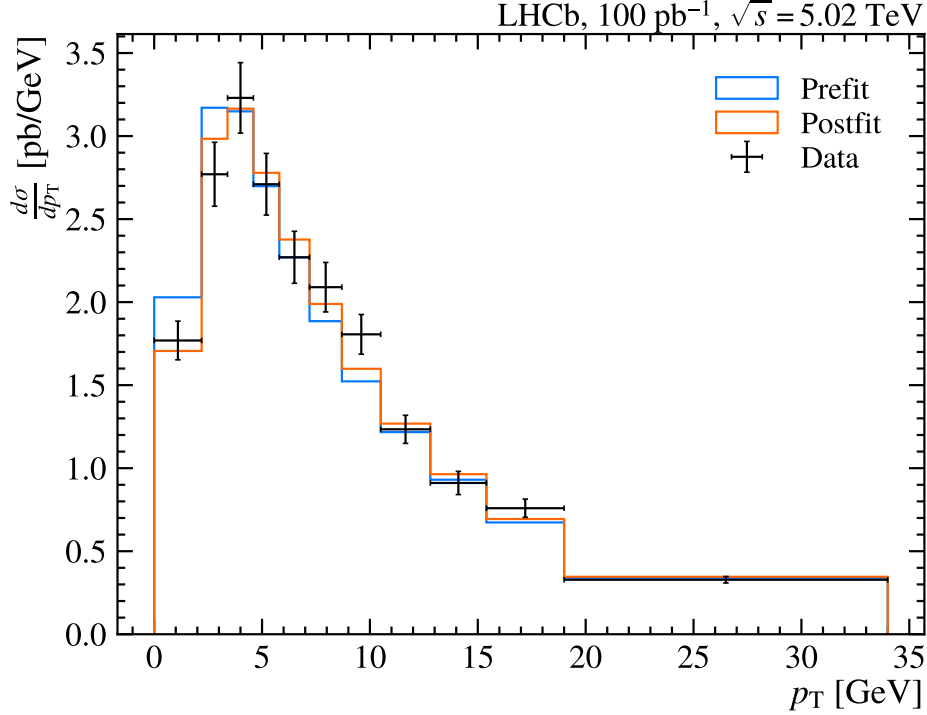
Figure 12: Differential cross-section data for Z-boson production from Ref. [3] compared to the physics model to be used in the m_W determination, before and after fitting for α_s and g.

Perturbative accuracy in the strong coupling: The error due to missing higher-order terms in the strong coupling α_s is assessed by varying the renormalisation and factorisation scales using the same prescription described for the MCFM predictions in Sec. 6. The resulting uncertainty is 14 MeV.

QED accuracy: As in Ref. [11], three additional m_W fits are performed. Each uses one of the three different models already described, rather than their average. The largest variation of 13 MeV is assigned as the uncertainty.

Parton distribution functions: Each of the three used PDF sets is provided with a prescription for assessing the uncertainty on an observable. For the NNPDF3.1 set this is based on taking the RMS of predictions computed with 100 different "replica" PDF sets. Eigenvectors are used for the uncertainties on the other two PDF sets. Assuming full correlation between the three PDF sets, the PDF uncertainty on the arithmetic average of the three is 22 MeV.

Table 3 lists the m_W fit results for the three different PDF sets. The variation in the three central values is smaller than, but comparable in size to, the PDF uncertainties for the three sets. The final quoted value of m_W is the average of the three values obtained by using the three sets of PDFs. The PDF uncertainty added to the overall theoretical uncertainty is calculated as an average of individual uncertainties for each set of PDFs. The final result is

$$m_W = 80369 \pm 130 \pm 33 \, \text{MeV},$$

18

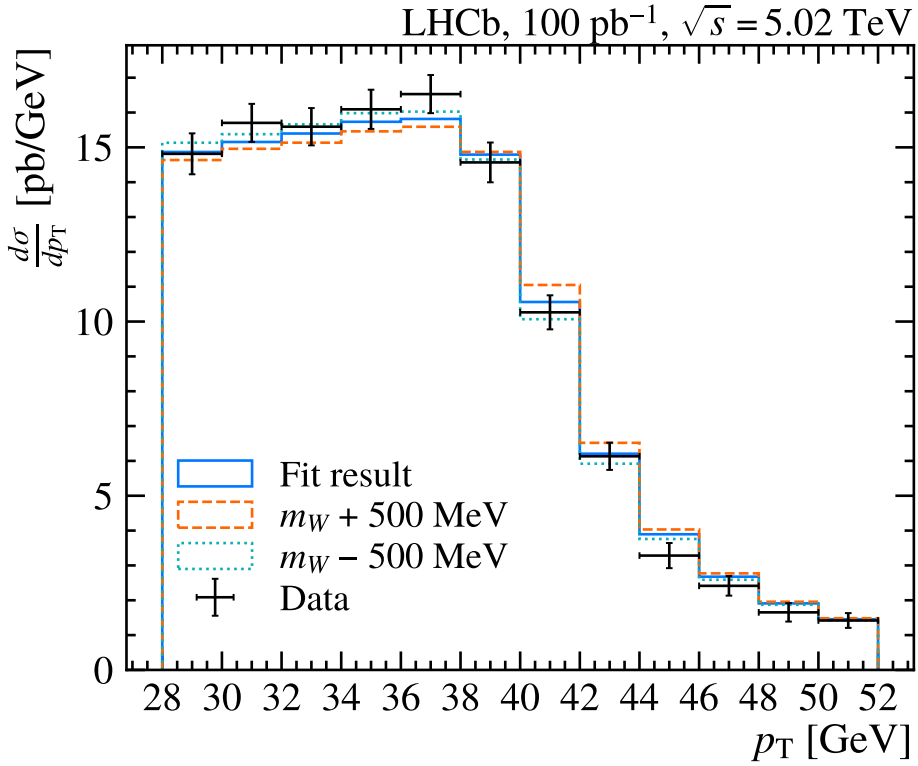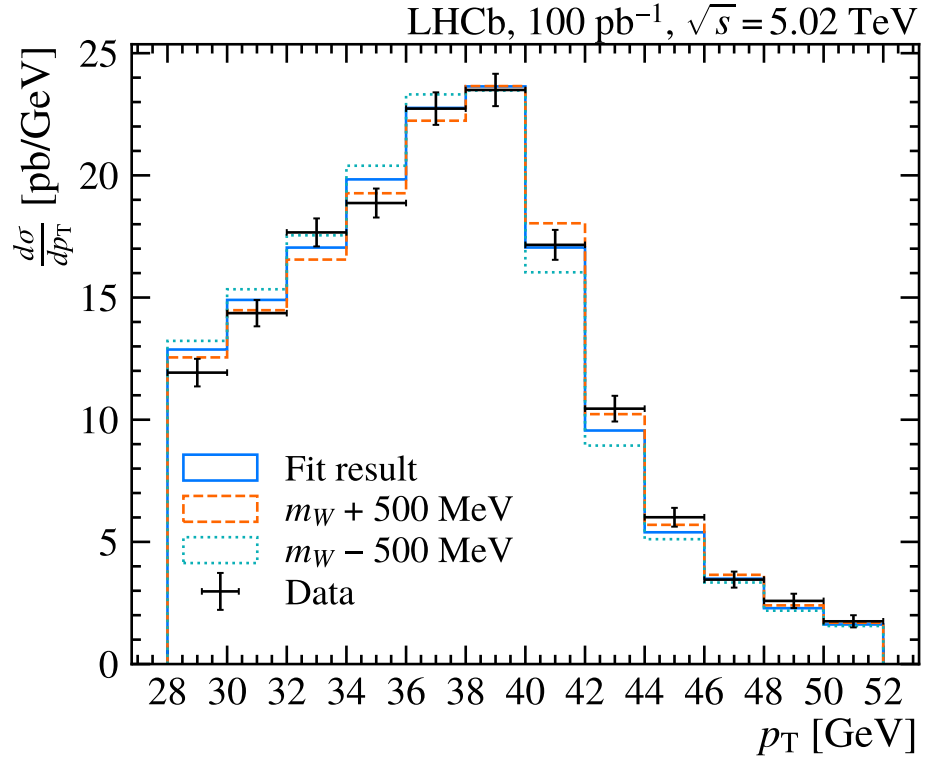Figure 13: Comparison of the (upper) W^+ and (lower) W^- $\mathrm{d}\sigma/\mathrm{d}p_\mathrm{T}$ data with the results of the m_W fit. The m_W fit results shifted by two extreme values of $\pm 500\,\mathrm{MeV}$ are also shown for illustration.

Table 3: Results of the m_W fit with the NNPDF3.1, MSHT20 and CT18 PDF sets. The m_W fit result includes the total covariance of the differential cross-section measurement. The theory uncertainty σ_{theory} includes all other sources except for the PDFs themselves.

PDF set	χ^2/ndf	m_W	σ_{theory}	σ_{PDF}
NNPDF3.1	25.6/21	$80366 \pm 130\,\text{MeV}$	$25\,\text{MeV}$	$28\,\text{MeV}$
MSHT20	27.2/21	$80380 \pm 129\,\text{MeV}$	$25\,\text{MeV}$	$15\,\text{MeV}$
CT18	23.9/21	$80362 \pm 130\,\text{MeV}$	$25\,\text{MeV}$	$23\,\text{MeV}$

Table 4: Impact of each source of experimental systematic uncertainty on the m_W uncertainty. The impact is defined as the square root of the difference in quadrature between the statistical uncertainty and the uncertainty including a single systematic source. The changes in the fit χ^2 and best-fit m_W values are also shown. The shift in the W-boson mass, denoted Δm_W, is defined as the value after the change minus the value before. Impacts or changes in the χ^2 of less than one unit are indicated with a dash.

Source	Impact [MeV]	$\Delta\chi^2$	Δm_W [MeV]
Charge-independent momentum biases	58	–	-8
Charge-dependent momentum biases	41	-19	-150
Hadronic background	7	-2	$+13$
Muon efficiency	15	-1	$+8$
Isolation	15	–	-3
Unfolding	–	-1	$+7$
Quadrature sum	75		

where the first uncertainty reflects experimental contributions, primarily from the measurement of $\mathrm{d}\sigma/\mathrm{d}p_{\mathrm{T}}$, and the second represents theoretical uncertainties. The latter is obtained by combining, in quadrature, the QCD and QED uncertainties together with the averaged PDF uncertainty. This result is compatible with earlier experimental measurements (see Sec. 1) and with the global electroweak fit [43].

All sources of uncertainty on the differential cross-section measurement are already accounted for in the "experimental" uncertainty of 130 MeV, through the total covariance of the measurement. However, it is informative to decompose the impact of the different sources of systematic uncertainty on the differential measurement. Table 4 lists, for each source of systematic uncertainty, the impact on the precision of the m_W fit result, defined as the quadrature difference in uncertainty when that source is included on its own, compared with the case where no uncertainty sources are included. The charge-independent momentum bias uncertainty has the largest impact, of 58 MeV. The next most important source is the charge-dependent momentum biases. When this uncertainty is removed from the fit, there is also a large shift in the best-fit m_W value; however, there is a corresponding large increase in χ^2, so the data have insufficient error coverage when this source is not included. The other two categories of uncertainty have impacts of 15 MeV or less. The statistical uncertainty on the measurement can be estimated by subtracting, in quadrature, the total uncertainty in Table 4 from the experimental uncertainty coming from the background subtraction fit, and amounts to about 106 MeV.

8 Cross-checks

The first set of cross-checks looks at the sensitivity of the measured m_W value to changes in the differential cross-section measurement.

Sensitivity to the m_W value in the simulation: The value of m_W in the signal simulation used to construct the response matrix is shifted by $+100\,\text{MeV}$. This results in a shift of only $-3\,\text{MeV}$ in the determination of m_W.

The W production model: The baseline result uses the PYTHIA8 description of the W-boson production. If the response matrix is constructed with the PYTHIA8 events weighted to match the unpolarised cross-section predictions of DYTURBO, the final value of m_W is shifted by $-6\,\text{MeV}$. If, instead, the angular distributions are weighted based on the angular coefficients of DYTURBO, the value of m_W is shifted by $17\,\text{MeV}$.

The second set of cross-checks considers variations only in the m_W fit.

Fit parameters: By default, the m_W fit uses the α_s value determined from the fit to the Z-boson data, but allows g to vary freely to a value preferred by the W-boson data. If the g value is also fixed to the larger value found in the fit to the Z-boson data, m_W shifts by $-58\,\text{MeV}$. If, instead, α_s is allowed to vary independently for the m_W fit, the shift in m_W is of $-1\,\text{MeV}$.

QCD scales: The baseline DYTURBO predictions are made with the renormalisation and factorisation scales parametrised as the quadrature sum of the dilepton mass and p_T. An alternative scheme, with the scales set to the dilepton mass, results in a shift in m_W of $-2\,\text{MeV}$.

QCD cut-off treatment: DYTURBO uses an inverse Bessel transform and has a default cut-off value of $3\,\text{GeV}$ that avoids the Landau pole. Changing the cut-off value to $1\,\text{GeV}$, the m_W value shifts by only $3\,\text{MeV}$.

Partial inclusion of higher orders: A DYTURBO prediction at N3LL and N3LO, with default values of α_s and g, is used to transform the baseline (N2LL and N2LO) predictions. This results in a shift in m_W of $-8\,\text{MeV}$.

PDF set: The three PDF sets used in the m_W determination are consistent with those used in previous LHCb analyses [11, 42]. The result with the NNPDF4.0 PDF set, which was not included, is shifted by $-5\,\text{MeV}$ compared to the result with the NNPDF3.1 PDF set.

In summary, the variations observed in all cross-checks are minor in relation to experimental and theoretical uncertainties and align with the baseline result. This agreement provides additional confidence in the robustness and reliability of the measurement.

9 Conclusion

This paper reports a measurement of the differential cross-section for $pp \to W^{\pm}(\to \mu^{\pm}\nu_\mu)X$ production in muon p_T intervals. For the first time, we demonstrate the feasibility of using such differential data in a subsequent determination of the W-boson mass.

The cross-sections are measured at a pp centre-of-mass energy of $\sqrt{s} = 5.02\,\text{TeV}$ using a limited dataset corresponding to an integrated luminosity of $100\,\text{pb}^{-1}$, recorded during 2017 by the LHCb experiment. Integrated over the muon pseudorapidity range $2.2 < \eta < 4.4$, the cross-sections are measured differentially in twelve intervals of muon transverse momentum in the range $28 < p_{\text{T}} < 52\,\text{GeV}$. The measured cross-sections integrated over p_{T} are

$$\sigma_{W^+ \to \mu^+ \nu_\mu} = 300.9 \pm 2.4 \pm 3.8 \pm 6.0\,\text{pb},$$
$$\sigma_{W^- \to \mu^- \bar{\nu}_\mu} = 236.9 \pm 2.1 \pm 2.7 \pm 4.7\,\text{pb},$$

where the first, second and third uncertainties are statistical, systematic and due to the luminosity determination, respectively. These results are consistent with theoretical predictions at fixed-order in the strong coupling. As a proof of principle, the differential results are used to determine the W-boson mass

$$m_W = 80369 \pm 130 \pm 33\,\text{MeV},$$

where the first uncertainty is experimental and the second is theoretical. This result is in agreement with earlier measurements and indirect determinations based on electroweak precision data. The analysis approach can be applied to the LHCb Run 2 dataset at $\sqrt{s} = 13\,\text{TeV}$, which contains roughly two orders of magnitude more W-boson decays than the small dataset analysed here, with an expected statistical uncertainty on m_W of around $12\,\text{MeV}$ as well as reduced systematic uncertainties. Looking ahead, it is expected that Run 3 data will provide improved precision, benefitting from increased statistics and improved detector performance.

Acknowledgements

Appendix

A   Total covariance matrix

The total covariance matrix (statistical + systematic) used to fit m_W, as demonstrated in Sec. 7, is given in Listing 1.

Listing 1: Full 24×24 covariance matrix of the measurement.

```
Row 1: 0.3192, -0.0252, 0.0287, 0.0302, 0.0696, 0.0258, 0.0048,
   -0.0028, -0.0022, 0.0057, 0.0089, -0.0050, 0.0644, 0.0592, 0.0113,
   0.0273, 0.0114, 0.0369, 0.0145, 0.0241, 0.0085, 0.0113, 0.0022,
   0.0114
Row 2: -0.0252, 0.2915, 0.0282, 0.0816, 0.0403, 0.0529, 0.0213,
   -0.0106, 0.0045, -0.0002, 0.0015, 0.0020, -0.0114, 0.0001, 0.0381,
   0.0029, 0.0381, 0.0154, 0.0314, 0.0140, 0.0197, -0.0010, 0.0031,
   0.0040
Row 3: 0.0287, 0.0282, 0.3286, 0.0106, 0.0850, 0.0457, 0.0209, -0.0029,
    0.0089, -0.0147, 0.0099, -0.0054, -0.0004, -0.0021, 0.0336, 0.0299,
    0.0458, -0.0015, 0.0531, 0.0150, -0.0105, 0.0169, 0.0179, -0.0033
Row 4: 0.0302, 0.0816, 0.0106, 0.3515, -0.0303, 0.0844, 0.0056,
   -0.0241, -0.0006, 0.0015, -0.0022, -0.0008, 0.0014, 0.0153, 0.0345,
   -0.0004, 0.0194, 0.0494, 0.0292, 0.0305, 0.0337, -0.0014, -0.0072,
   0.0130
Row 5: 0.0696, 0.0403, 0.0850, -0.0303, 0.4428, -0.0743, 0.0321,
   -0.0000, 0.0002, -0.0148, 0.0177, -0.0147, 0.0379, 0.0265, 0.0118,
   0.0579, 0.0541, -0.0048, 0.0592, 0.0192, -0.0229, 0.0290, 0.0242,
   -0.0030
Row 6: 0.0258, 0.0529, 0.0457, 0.0844, -0.0743, 0.4385, -0.0656,
   0.0415, 0.0123, 0.0194, -0.0072, 0.0159, 0.0193, 0.0311, 0.0482,
   0.0126, 0.0219, 0.0682, 0.0057, 0.0229, 0.0290, -0.0085, -0.0087,
   0.0094
Row 7: 0.0048, 0.0213, 0.0209, 0.0056, 0.0321, -0.0656, 0.3750,
   -0.0223, 0.0530, 0.0155, 0.0182, 0.0112, 0.0240, 0.0266, 0.0404,
   0.0286, 0.0448, 0.0119, 0.0058, -0.0103, -0.0045, 0.0030, -0.0004,
   -0.0018
Row 8: -0.0028, -0.0106, -0.0029, -0.0241, -0.0000, 0.0415, -0.0223,
   0.2770, -0.0277, 0.0308, 0.0010, 0.0233, 0.0285, 0.0214, 0.0132,
   0.0504, 0.0237, -0.0041, -0.0066, -0.0147, -0.0299, 0.0055, 0.0153,
   -0.0130
Row 9: -0.0022, 0.0045, 0.0089, -0.0006, 0.0002, 0.0123, 0.0530,
   -0.0277, 0.1482, -0.0384, 0.0187, 0.0070, 0.0084, 0.0127, 0.0200,
   0.0142, 0.0166, 0.0035, -0.0013, -0.0059, -0.0054, -0.0013, 0.0001,
   -0.0025
Row 10: 0.0057, -0.0002, -0.0147, 0.0015, -0.0148, 0.0194, 0.0155,
   0.0308, -0.0384, 0.1077, -0.0402, 0.0196, 0.0122, 0.0184, 0.0116,
   -0.0035, 0.0001, 0.0253, -0.0176, -0.0028, 0.0147, -0.0091, -0.0094,
    0.0027
Row 11: 0.0089, 0.0015, 0.0099, -0.0022, 0.0177, -0.0072, 0.0182,
   0.0010, 0.0187, -0.0402, 0.0861, -0.0373, 0.0032, 0.0024, 0.0041,
   0.0054, 0.0116, -0.0060, 0.0081, -0.0031, -0.0080, 0.0082, 0.0002,
   0.0016
Row 12: -0.0050, 0.0020, -0.0054, -0.0008, -0.0147, 0.0159, 0.0112,
   0.0233, 0.0070, 0.0196, -0.0373, 0.0622, 0.0022, 0.0076, 0.0074,
   0.0086, 0.0020, 0.0048, -0.0091, -0.0012, -0.0006, -0.0062, 0.0032,
   -0.0037
```

Row 13: 0.0644, -0.0114, -0.0004, 0.0014, 0.0379, 0.0193, 0.0240,
    0.0285, 0.0084, 0.0122, 0.0032, 0.0022, 0.3450, 0.0221, 0.0260,
    0.0366, 0.0104, 0.0121, -0.0080, -0.0013, -0.0097, 0.0020, 0.0013,
    -0.0078
Row 14: 0.0592, 0.0001, -0.0021, 0.0153, 0.0265, 0.0311, 0.0266,
    0.0214, 0.0127, 0.0184, 0.0024, 0.0076, 0.0221, 0.2980, -0.0223,
    0.0307, 0.0159, 0.0461, -0.0091, 0.0065, 0.0146, -0.0049, -0.0084,
    0.0063
Row 15: 0.0113, 0.0381, 0.0336, 0.0345, 0.0118, 0.0482, 0.0404, 0.0132,
    0.0200, 0.0116, 0.0041, 0.0074, 0.0260, -0.0223, 0.2866, -0.0498,
    0.0421, 0.0300, -0.0034, -0.0039, 0.0182, -0.0098, -0.0058, 0.0017
Row 16: 0.0273, 0.0029, 0.0299, -0.0004, 0.0579, 0.0126, 0.0286,
    0.0504, 0.0142, -0.0035, 0.0054, 0.0086, 0.0366, 0.0307, -0.0498,
    0.3167, -0.0313, -0.0023, 0.0290, -0.0008, -0.0384, 0.0222, 0.0284,
    -0.0135
Row 17: 0.0114, 0.0381, 0.0458, 0.0194, 0.0541, 0.0219, 0.0448, 0.0237,
    0.0166, 0.0001, 0.0116, 0.0020, 0.0104, 0.0159, 0.0421, -0.0313,
    0.2996, -0.0709, 0.0469, -0.0004, -0.0087, 0.0107, 0.0142, -0.0042
Row 18: 0.0369, 0.0154, -0.0015, 0.0494, -0.0048, 0.0682, 0.0119,
    -0.0041, 0.0035, 0.0253, -0.0060, 0.0048, 0.0121, 0.0461, 0.0300,
    -0.0023, -0.0709, 0.3263, -0.0814, 0.0406, 0.0487, -0.0131, -0.0306,
    0.0233
Row 19: 0.0145, 0.0314, 0.0531, 0.0292, 0.0592, 0.0057, 0.0058,
    -0.0066, -0.0013, -0.0176, 0.0081, -0.0091, -0.0080, -0.0091,
    -0.0034, 0.0290, 0.0469, -0.0814, 0.2389, -0.0289, -0.0062, 0.0223,
    0.0220, -0.0016
Row 20: 0.0241, 0.0140, 0.0150, 0.0305, 0.0192, 0.0229, -0.0103,
    -0.0147, -0.0059, -0.0028, -0.0031, -0.0012, -0.0013, 0.0065,
    -0.0039, -0.0008, -0.0004, 0.0406, -0.0289, 0.1525, -0.0253, 0.0181,
    -0.0035, 0.0109
Row 21: 0.0085, 0.0197, -0.0105, 0.0337, -0.0229, 0.0290, -0.0045,
    -0.0299, -0.0054, 0.0147, -0.0080, -0.0006, -0.0097, 0.0146, 0.0182,
    -0.0384, -0.0087, 0.0487, -0.0062, -0.0253, 0.1302, -0.0491,
    -0.0178, 0.0162
Row 22: 0.0113, -0.0010, 0.0169, -0.0014, 0.0290, -0.0085, 0.0030,
    0.0055, -0.0013, -0.0091, 0.0082, -0.0062, 0.0020, -0.0049, -0.0098,
    0.0222, 0.0107, -0.0131, 0.0223, 0.0181, -0.0491, 0.0790, -0.0109,
    0.0035
Row 23: 0.0022, 0.0031, 0.0179, -0.0072, 0.0242, -0.0087, -0.0004,
    0.0153, 0.0001, -0.0094, 0.0002, 0.0032, 0.0013, -0.0084, -0.0058,
    0.0284, 0.0142, -0.0306, 0.0220, -0.0035, -0.0178, -0.0109, 0.0702,
    -0.0306
Row 24: 0.0114, 0.0040, -0.0033, 0.0130, -0.0030, 0.0094, -0.0018,
    -0.0130, -0.0025, 0.0027, 0.0016, -0.0037, -0.0078, 0.0063, 0.0017,
    -0.0135, -0.0042, 0.0233, -0.0016, 0.0109, 0.0162, 0.0035, -0.0306,
    0.0451

References

[1] LHCb collaboration, A. A. Alves Jr. *et al.*, *The LHCb detector at the LHC*, JINST **3** (2008) S08005.

[2] LHCb collaboration, R. Aaij *et al.*, *LHCb detector performance*, Int. J. Mod. Phys. **A30** (2015) 1530022, arXiv:1412.6352.

[3] LHCb collaboration, R. Aaij *et al.*, *Measurement of the Z boson production cross-section at 5.02 TeV*, JHEP **02** (2024) 070, arXiv:2308.12940.

[4] LHCb collaboration, R. Aaij *et al.*, *Measurement of the forward Z boson cross-section in pp collisions at $\sqrt{s} = 7$ TeV*, JHEP **08** (2015) 039, arXiv:1505.07024.

[5] LHCb collaboration, R. Aaij *et al.*, *Measurement of forward W and Z boson production in pp collisions at $\sqrt{s} = 8$ TeV*, JHEP **01** (2016) 155, arXiv:1511.08039.

[6] LHCb collaboration, R. Aaij *et al.*, *Precision measurement of forward Z boson production in proton-proton collisions at $\sqrt{s} = 13$ TeV*, JHEP **07** (2022) 026, arXiv:2112.07458.

[7] LHCb collaboration, R. Aaij *et al.*, *Measurement of the forward W boson production cross-section in pp collisions at $\sqrt{s} = 7$ TeV*, JHEP **12** (2014) 079, arXiv:1408.4354.

[8] ALEPH, DELPHI, L3, OPAL, LEP Electroweak collaboration, S. Schael *et al.*, *Electroweak measurements in electron-positron collisions at W-boson-pair energies at LEP*, Phys. Rept. **532** (2013) 119, arXiv:1302.3415.

[9] CMS collaboration, A. M. Sirunyan, A. Tumasyan, W. Adam *et al.*, *High-precision measurement of the W boson mass with the CMS experiment at the LHC*, arXiv:2412.13872, submitted for publication in Nature.

[10] ATLAS collaboration, G. Aad *et al.*, *Measurement of the W-boson mass and width with the ATLAS detector using proton-proton collisions at $\sqrt{s} = 7$ TeV*, Eur. Phys. J. **C84** (2024) 1309, arXiv:2403.15085.

[11] LHCb collaboration, R. Aaij *et al.*, *Measurement of the W boson mass*, JHEP **01** (2022) 036, arXiv:2109.01113.

[12] CDF collaboration, T. Aaltonen *et al.*, *High-precision measurement of the W-boson mass with the CDF II detector*, Science **376** (2022) 170.

[13] D0 collaboration, V. M. Abazov *et al.*, *Measurement of the W boson mass with the D0 detector*, Phys. Rev. Lett. **108** (2012) 151804, arXiv:1203.0293.

[14] LHC-TeV MW Working Group, S. Amoroso *et al.*, *Compatibility and combination of world W-boson mass measurements*, Eur. Phys. J. **C84** (2024) 451, arXiv:2308.09417.

[15] CMS collaboration, A. M. Sirunyan *et al.*, *Measurements of the W boson rapidity, helicity, double-differential cross sections, and charge asymmetry in pp collisions at $\sqrt{s} = 13$ TeV*, Phys. Rev. **D102** (2020) 092012, arXiv:2008.04174.

[16] ATLAS collaboration, G. Aad *et al.*, *Measurement of $W^{\pm}$-boson differential cross-sections in proton-proton collisions with low pile-up data at $\sqrt{s} = 5.02$ TeV and 13 TeV with the ATLAS detector*, Eur. Phys. J. **C85** (2025) 729, `arXiv:2502.09403`.

[17] LHCb collaboration, R. Aaij *et al.*, *Precision luminosity measurements at LHCb*, JINST **9** (2014) P12005, `arXiv:1410.0149`.

[18] R. Aaij *et al.*, *Performance of the LHCb Vertex Locator*, JINST **9** (2014) P09007, `arXiv:1405.7808`.

[19] P. d'Argent *et al.*, *Improved performance of the LHCb Outer Tracker in LHC Run 2*, JINST **12** (2017) P11016, `arXiv:1708.00819`.

[20] A. A. Alves Jr. *et al.*, *Performance of the LHCb muon system*, JINST **8** (2013) P02022, `arXiv:1211.1346`.

[21] R. Aaij *et al.*, *Design and performance of the LHCb trigger and full real-time reconstruction in Run 2 of the LHC*, JINST **14** (2019) P04013, `arXiv:1812.10790`.

[22] T. Sjöstrand, S. Mrenna, and P. Skands, *A brief introduction to PYTHIA 8.1*, Comput. Phys. Commun. **178** (2008) 852, `arXiv:0710.3820`.

[23] I. Belyaev *et al.*, *Handling of the generation of primary events in Gauss, the LHCb simulation framework*, J. Phys. Conf. Ser. **331** (2011) 032047.

[24] D. J. Lange, *The EvtGen particle decay simulation package*, Nucl. Instrum. Meth. **A462** (2001) 152.

[25] N. Davidson, T. Przedzinski, and Z. Was, *PHOTOS interface in C++: Technical and physics documentation*, Comp. Phys. Comm. **199** (2016) 86, `arXiv:1011.0937`.

[26] Geant4 collaboration, J. Allison *et al.*, *Geant4 developments and applications*, IEEE Trans. Nucl. Sci. **53** (2006) 270; Geant4 collaboration, S. Agostinelli *et al.*, *Geant4: A simulation toolkit*, Nucl. Instrum. Meth. **A506** (2003) 250.

[27] M. Clemencic *et al.*, *The LHCb simulation application, Gauss: Design, evolution and experience*, J. Phys. Conf. Ser. **331** (2011) 032023.

[28] W. Barter, M. Pili, and M. Vesterinen, *A simple method to determine charge-dependent curvature biases in track reconstruction in hadron collider experiments*, Eur. Phys. J. **C81** (2021) 251, `arXiv:2101.05675`.

[29] LHCb collaboration, R. Aaij *et al.*, *Curvature-bias corrections using a pseudomass method*, JINST **19** (2024) P03010, `arXiv:2311.04670`.

[30] R. J. Barlow and C. Beeston, *Fitting using finite Monte Carlo samples*, Comput. Phys. Commun. **77** (1993) 219.

[31] J. S. Conway, *Incorporating nuisance parameters in likelihoods for multisource spectra*, in *Proceedings of the PHYSTAT 2011 Workshop*, 115–120, 2011, `arXiv:1103.0354`.

[32] J. Campbell and T. Neumann, *Precision phenomenology with MCFM*, JHEP **12** (2019) 034, `arXiv:1909.09117`.

[33] LHCb collaboration, R. Aaij *et al.*, *Measurement of prompt hadron production ratios in pp collisions at $\sqrt{s} = 0.9$ and 7 TeV*, Eur. Phys. J. **C72** (2012) 2168, arXiv:1206.5160.

[34] T.-J. Hou *et al.*, *New CTEQ global analysis of quantum chromodynamics with high-precision data from the LHC*, Phys. Rev. D **103** (2021) 014013, arXiv:1912.10053.

[35] NNPDF collaboration, R. D. Ball *et al.*, *Parton distributions from high-precision collider data*, Eur. Phys. J. C **77** (2017) 663, arXiv:1706.00428.

[36] NNPDF collaboration, R. D. Ball *et al.*, *The path to proton structure at 1% accuracy*, Eur. Phys. J. **C82** (2022) 428, arXiv:2109.02653.

[37] S. Bailey *et al.*, *Parton distributions from LHC, HERA, Tevatron and fixed target data: MSHT20 PDFs*, arXiv:2012.04684.

[38] K. Hamilton, P. Nason, and G. Zanderighi, *MINLO: Multi-Scale Improved NLO*, JHEP **10** (2012) 155, arXiv:1206.3572.

[39] J. Bellm *et al.*, *Herwig 7.0/Herwig++ 3.0 release note*, Eur. Phys. J. **C76** (2016) 196, arXiv:1512.01178.

[40] J. C. Collins and D. E. Soper, *Angular distribution of dileptons in high-energy hadron collisions*, Phys. Rev. **D16** (1977) 2219.

[41] S. Camarda *et al.*, *DYTurbo: fast predictions for Drell–Yan processes*, Eur. Phys. J. **C80** (2020) 251, Erratum ibid. **C80** (2020) 440, arXiv:1910.07049.

[42] LHCb collaboration, R. Aaij *et al.*, *Measurement of the effective leptonic weak mixing angle*, JHEP **12** (2024) 026, arXiv:2410.02502.

[43] J. Haller *et al.*, *Update of the global electroweak fit and constraints on two-Higgs-doublet models*, Eur. Phys. J. **C78** (2018) 675, arXiv:1803.01853.

LHCb collaboration

R. Aaij[38] ⓘ, A.S.W. Abdelmotteleb[57] ⓘ, C. Abellan Beteta[51] ⓘ, F. Abudinén[57] ⓘ,
T. Ackernley[61] ⓘ, A. A. Adefisoye[69] ⓘ, B. Adeva[47] ⓘ, M. Adinolfi[55] ⓘ, P. Adlarson[85] ⓘ,
C. Agapopoulou[14] ⓘ, C.A. Aidala[87] ⓘ, Z. Ajaltouni[11], S. Akar[11] ⓘ, K. Akiba[38] ⓘ,
P. Albicocco[28] ⓘ, J. Albrecht[19,g] ⓘ, R. Aleksiejunas[80] ⓘ, F. Alessio[49] ⓘ,
P. Alvarez Cartelle[56] ⓘ, R. Amalric[16] ⓘ, S. Amato[3] ⓘ, J.L. Amey[55] ⓘ, Y. Amhis[14] ⓘ,
L. An[6] ⓘ, L. Anderlini[27] ⓘ, M. Andersson[51] ⓘ, P. Andreola[51] ⓘ, M. Andreotti[26] ⓘ, S.
Andres Estrada[84] ⓘ, A. Anelli[31,p,49] ⓘ, D. Ao[7] ⓘ, C. Arata[12] ⓘ, F. Archilli[37,w] ⓘ, Z. Areg[69] ⓘ,
M. Argenton[26] ⓘ, S. Arguedas Cuendis[9,49] ⓘ, L. Arnone[31,p] ⓘ, A. Artamonov[44] ⓘ,
M. Artuso[69] ⓘ, E. Aslanides[13] ⓘ, R. Ataíde Da Silva[50] ⓘ, M. Atzeni[65] ⓘ, B. Audurier[12] ⓘ, J.
A. Authier[15] ⓘ, D. Bacher[64] ⓘ, I. Bachiller Perea[50] ⓘ, S. Bachmann[22] ⓘ, M. Bachmayer[50] ⓘ,
J.J. Back[57] ⓘ, P. Baladron Rodriguez[47] ⓘ, V. Balagura[15] ⓘ, A. Balboni[26] ⓘ, W. Baldini[26] ⓘ,
Z. Baldwin[78] ⓘ, L. Balzani[19] ⓘ, H. Bao[7] ⓘ, J. Baptista de Souza Leite[2] ⓘ,
C. Barbero Pretel[47,12] ⓘ, M. Barbetti[27] ⓘ, I. R. Barbosa[70] ⓘ, R.J. Barlow[63] ⓘ,
M. Barnyakov[25] ⓘ, S. Barsuk[14] ⓘ, W. Barter[59] ⓘ, J. Bartz[69] ⓘ, S. Bashir[40] ⓘ, B. Batsukh[5] ⓘ,
P. B. Battista[14] ⓘ, A. Bay[50] ⓘ, A. Beck[65] ⓘ, M. Becker[19] ⓘ, F. Bedeschi[35] ⓘ,
I.B. Bediaga[2] ⓘ, N. A. Behling[19] ⓘ, S. Belin[47] ⓘ, A. Bellavista[25] ⓘ, K. Belous[44] ⓘ,
I. Belov[29] ⓘ, I. Belyaev[36] ⓘ, G. Benane[13] ⓘ, G. Bencivenni[28] ⓘ, E. Ben-Haim[16] ⓘ,
A. Berezhnoy[44] ⓘ, R. Bernet[51] ⓘ, S. Bernet Andres[46] ⓘ, A. Bertolin[33] ⓘ, C. Betancourt[51] ⓘ,
F. Betti[59] ⓘ, J. Bex[56] ⓘ, Ia. Bezshyiko[51] ⓘ, O. Bezshyyko[86] ⓘ, J. Bhom[41] ⓘ, M.S. Bieker[18] ⓘ,
N.V. Biesuz[26] ⓘ, P. Billoir[16] ⓘ, A. Biolchini[38] ⓘ, M. Birch[62] ⓘ, F.C.R. Bishop[10] ⓘ,
A. Bitadze[63] ⓘ, A. Bizzeti[27,q] ⓘ, T. Blake[57,c] ⓘ, F. Blanc[50] ⓘ, J.E. Blank[19] ⓘ, S. Blusk[69] ⓘ,
V. Bocharnikov[44] ⓘ, J.A. Boelhauve[19] ⓘ, O. Boente Garcia[15] ⓘ, T. Boettcher[68] ⓘ, A.
Bohare[59] ⓘ, A. Boldyrev[44] ⓘ, C.S. Bolognani[82] ⓘ, R. Bolzonella[26,m] ⓘ, R. B. Bonacci[1] ⓘ,
N. Bondar[44,49] ⓘ, A. Bordelius[49] ⓘ, F. Borgato[33,49] ⓘ, S. Borghi[63] ⓘ, M. Borsato[31,p] ⓘ,
J.T. Borsuk[83] ⓘ, E. Bottalico[61] ⓘ, S.A. Bouchiba[50] ⓘ, M. Bovill[64] ⓘ, T.J.V. Bowcock[61] ⓘ,
A. Boyer[49] ⓘ, C. Bozzi[26] ⓘ, J. D. Brandenburg[88] ⓘ, A. Brea Rodriguez[50] ⓘ, N. Breer[19] ⓘ,
J. Brodzicka[41] ⓘ, A. Brossa Gonzalo[47,†] ⓘ, J. Brown[61] ⓘ, D. Brundu[32] ⓘ, E. Buchanan[59] ⓘ, M.
Burgos Marcos[82] ⓘ, A.T. Burke[63] ⓘ, C. Burr[49] ⓘ, C. Buti[27] ⓘ, J.S. Butter[56] ⓘ,
J. Buytaert[49] ⓘ, W. Byczynski[49] ⓘ, S. Cadeddu[32] ⓘ, H. Cai[75], Y. Cai[5] ⓘ, A. Caillet[16],
R. Calabrese[26,m] ⓘ, S. Calderon Ramirez[9] ⓘ, L. Calefice[45] ⓘ, M. Calvi[31,p] ⓘ,
M. Calvo Gomez[46] ⓘ, P. Camargo Magalhaes[2,a] ⓘ, J. I. Cambon Bouzas[47] ⓘ, P. Campana[28] ⓘ,
D.H. Campora Perez[82] ⓘ, A.F. Campoverde Quezada[7] ⓘ, S. Capelli[31] ⓘ, M. Caporale[25] ⓘ,
L. Capriotti[26] ⓘ, R. Caravaca-Mora[9] ⓘ, A. Carbone[25,k] ⓘ, L. Carcedo Salgado[47] ⓘ,
R. Cardinale[29,n] ⓘ, A. Cardini[32] ⓘ, P. Carniti[31] ⓘ, L. Carus[22], A. Casais Vidal[65] ⓘ,
R. Caspary[22] ⓘ, G. Casse[61] ⓘ, M. Cattaneo[49] ⓘ, G. Cavallero[26] ⓘ, V. Cavallini[26,m] ⓘ,
S. Celani[22] ⓘ, I. Celestino[35,t] ⓘ, S. Cesare[30,o] ⓘ, A.J. Chadwick[61] ⓘ, I. Chahrour[87] ⓘ, H.
Chang[4,d] ⓘ, M. Charles[16] ⓘ, Ph. Charpentier[49] ⓘ, E. Chatzianagnostou[38] ⓘ, R. Cheaib[79] ⓘ,
M. Chefdeville[10] ⓘ, C. Chen[56] ⓘ, J. Chen[50] ⓘ, S. Chen[5] ⓘ, Z. Chen[7] ⓘ, M. Cherif[12] ⓘ,
A. Chernov[41] ⓘ, S. Chernyshenko[53] ⓘ, X. Chiotopoulos[82] ⓘ, V. Chobanova[84] ⓘ,
M. Chrzaszcz[41] ⓘ, A. Chubykin[44] ⓘ, V. Chulikov[28,36,49] ⓘ, P. Ciambrone[28] ⓘ,
X. Cid Vidal[47] ⓘ, G. Ciezarek[49] ⓘ, P. Cifra[38] ⓘ, P.E.L. Clarke[59] ⓘ, M. Clemencic[49] ⓘ,
H.V. Cliff[56] ⓘ, J. Closier[49] ⓘ, C. Cocha Toapaxi[22] ⓘ, V. Coco[49] ⓘ, J. Cogan[13] ⓘ,
E. Cogneras[11] ⓘ, L. Cojocariu[43] ⓘ, S. Collaviti[50] ⓘ, P. Collins[49] ⓘ, T. Colombo[49] ⓘ,
M. Colonna[19] ⓘ, A. Comerma-Montells[45] ⓘ, L. Congedo[24] ⓘ, J. Connaughton[57] ⓘ,
A. Contu[32] ⓘ, N. Cooke[60] ⓘ, G. Cordova[35,t] ⓘ, C. Coronel[66] ⓘ, I. Corredoira[12] ⓘ,
A. Correia[16] ⓘ, G. Corti[49] ⓘ, J. Cottee Meldrum[55] ⓘ, B. Couturier[49] ⓘ, D.C. Craik[51] ⓘ,
M. Cruz Torres[2,h] ⓘ, E. Curras Rivera[50] ⓘ, R. Currie[59] ⓘ, C.L. Da Silva[68] ⓘ, S. Dadabaev[44] ⓘ,
L. Dai[72] ⓘ, X. Dai[4] ⓘ, E. Dall'Occo[49] ⓘ, J. Dalseno[84] ⓘ, C. D'Ambrosio[62] ⓘ, J. Daniel[11] ⓘ,

P. d'Argent[24], G. Darze[3], A. Davidson[57], J.E. Davies[63], O. De Aguiar Francisco[63],
C. De Angelis[32,l], F. De Benedetti[49], J. de Boer[38], K. De Bruyn[81], S. De Capua[63],
M. De Cian[63,49], U. De Freitas Carneiro Da Graca[2,b], E. De Lucia[28],
J.M. De Miranda[2], L. De Paula[3], M. De Serio[24,i], P. De Simone[28], F. De Vellis[19],
J.A. de Vries[82], F. Debernardis[24], D. Decamp[10], S. Dekkers[1], L. Del Buono[16],
B. Delaney[65], H.-P. Dembinski[19], J. Deng[8], V. Denysenko[51], O. Deschamps[11],
F. Dettori[32,l], B. Dey[79], P. Di Nezza[28], I. Diachkov[44], S. Didenko[44], S. Ding[69],
Y. Ding[50], L. Dittmann[22], V. Dobishuk[53], A. D. Docheva[60], A. Doheny[57],
C. Dong[4,d], A.M. Donohoe[23], F. Dordei[32], A.C. dos Reis[2], A. D. Dowling[69],
L. Dreyfus[13], W. Duan[73], P. Duda[83], L. Dufour[49], V. Duk[34], P. Durante[49], M.
M. Duras[83], J.M. Durham[68], O. D. Durmus[79], A. Dziurda[41], A. Dzyuba[44],
S. Easo[58], E. Eckstein[18], U. Egede[1], A. Egorychev[44], V. Egorychev[44],
S. Eisenhardt[59], E. Ejopu[61], L. Eklund[85], M. Elashri[66], J. Ellbracht[19], S. Ely[62],
A. Ene[43], J. Eschle[69], S. Esen[22], T. Evans[38], F. Fabiano[32], S. Faghih[66],
L.N. Falcao[2], B. Fang[7], R. Fantechi[35], L. Fantini[34,s], M. Faria[50], K. Farmer[59],
D. Fazzini[31,p], L. Felkowski[83], M. Feng[5,7], M. Feo[19], A. Fernandez Casani[48],
M. Fernandez Gomez[47], A.D. Fernez[67], F. Ferrari[25,k], F. Ferreira Rodrigues[3],
M. Ferrillo[51], M. Ferro-Luzzi[49], S. Filippov[44], R.A. Fini[24], M. Fiorini[26,m],
M. Firlej[40], K.L. Fischer[64], D.S. Fitzgerald[87], C. Fitzpatrick[63], T. Fiutowski[40],
F. Fleuret[15], A. Fomin[52], M. Fontana[25], L. F. Foreman[63], R. Forty[49],
D. Foulds-Holt[59], V. Franco Lima[3], M. Franco Sevilla[67], M. Frank[49],
E. Franzoso[26,m], G. Frau[63], C. Frei[49], D.A. Friday[63,49], J. Fu[7], Q. Führing[19,g,56],
T. Fulghesu[13], G. Galati[24], M.D. Galati[38], A. Gallas Torreira[47], D. Galli[25,k],
S. Gambetta[59], M. Gandelman[3], P. Gandini[30], B. Ganie[63], H. Gao[7], R. Gao[64],
T.Q. Gao[56], Y. Gao[8], Y. Gao[6], Y. Gao[8], L.M. Garcia Martin[50],
P. Garcia Moreno[45], J. García Pardiñas[65], P. Gardner[67], K. G. Garg[8],
L. Garrido[45], C. Gaspar[49], A. Gavrikov[33], L.L. Gerken[19], E. Gersabeck[20],
M. Gersabeck[20], T. Gershon[57], S. Ghizzo[29,n], Z. Ghorbanimoghaddam[55], F.
I. Giasemis[16,f], V. Gibson[56], H.K. Giemza[42], A.L. Gilman[66], M. Giovannetti[28],
A. Gioventù[45], L. Girardey[63,58], M.A. Giza[41], F.C. Glaser[14,22], V.V. Gligorov[16],
C. Göbel[70], L. Golinka-Bezshyyko[86], E. Golobardes[46], D. Golubkov[44],
A. Golutvin[62,49], S. Gomez Fernandez[45], W. Gomulka[40], I. Gonçales Vaz[49],
F. Goncalves Abrantes[64], M. Goncerz[41], G. Gong[4,d], J. A. Gooding[19],
I.V. Gorelov[44], C. Gotti[31], E. Govorkova[65], J.P. Grabowski[30],
L.A. Granado Cardoso[49], E. Graugés[45], E. Graverini[50,u], L. Grazette[57],
G. Graziani[27], A. T. Grecu[43], N.A. Grieser[66], L. Grillo[60], S. Gromov[44], C. Gu[15],
M. Guarise[26], L. Guerry[11], V. Guliaeva[44], P. A. Günther[22], A.-K. Guseinov[50],
E. Gushchin[44], Y. Guz[6,49], T. Gys[49], K. Habermann[18], T. Hadavizadeh[1],
C. Hadjivasiliou[67], G. Haefeli[50], C. Haen[49], S. Haken[56], G. Hallett[57],
P.M. Hamilton[67], J. Hammerich[61], Q. Han[33], X. Han[22,49],
S. Hansmann-Menzemer[22], L. Hao[7], N. Harnew[64], T. H. Harris[1], M. Hartmann[14],
S. Hashmi[40], J. He[7,e], A. Hedes[63], F. Hemmer[49], C. Henderson[66],
R. Henderson[14], R.D.L. Henderson[1], A.M. Hennequin[49], K. Hennessy[61],
L. Henry[50], J. Herd[62], P. Herrero Gascon[22], J. Heuel[17], A. Heyn[13], A. Hicheur[3],
G. Hijano Mendizabal[51], J. Horswill[63], R. Hou[8], Y. Hou[11], D. C. Houston[60],
N. Howarth[61], J. Hu[73], W. Hu[7], X. Hu[4,d], W. Hulsbergen[38], R.J. Hunter[57],
M. Hushchyn[44], D. Hutchcroft[61], M. Idzik[40], D. Ilin[44], P. Ilten[66], A. Iniukhin[44],
A. Iohner[10], A. Ishteev[44], K. Ivshin[44], H. Jage[17], S.J. Jaimes Elles[77,48,49],
S. Jakobsen[49], E. Jans[38], B.K. Jashal[48], A. Jawahery[67], C. Jayaweera[54],
V. Jevtic[19], Z. Jia[16], E. Jiang[67], X. Jiang[5,7], Y. Jiang[7], Y. J. Jiang[6],

E. Jimenez Moya[9] , N. Jindal[88] , M. John[64] , A. John Rubesh Rajan[23] ,
D. Johnson[54] , C.R. Jones[56] , S. Joshi[42] , B. Jost[49] , J. Juan Castella[56] , N. Jurik[49] ,
I. Juszczak[41] , D. Kaminaris[50] , S. Kandybei[52] , M. Kane[59] , Y. Kang[4,d] , C. Kar[11] ,
M. Karacson[49] , A. Kauniskangas[50] , J.W. Kautz[66] , M.K. Kazanecki[41] , F. Keizer[49] ,
M. Kenzie[56] , T. Ketel[38] , B. Khanji[69] , A. Kharisova[44] , S. Kholodenko[62,49] ,
G. Khreich[14] , T. Kirn[17] , V.S. Kirsebom[31,p] , O. Kitouni[65] , S. Klaver[39] ,
N. Kleijne[35,t] , D. K. Klekots[86] , K. Klimaszewski[42] , M.R. Kmiec[42] , T. Knospe[19] ,
R. Kolb[22] , S. Koliiev[53] , L. Kolk[19] , A. Konoplyannikov[6] , P. Kopciewicz[49] ,
P. Koppenburg[38] , A. Korchin[52] , M. Korolev[44] , I. Kostiuk[38] , O. Kot[53] ,
S. Kotriakhova , E. Kowalczyk[67] , A. Kozachuk[44] , P. Kravchenko[44] , L. Kravchuk[44] ,
O. Kravcov[80] , M. Kreps[57] , P. Krokovny[44] , W. Krupa[69] , W. Krzemien[42] ,
O. Kshyvanskyi[53] , S. Kubis[83] , M. Kucharczyk[41] , V. Kudryavtsev[44] , E. Kulikova[44] ,
A. Kupsc[85] , V. Kushnir[52] , B. Kutsenko[13] , J. Kvapil[68] , I. Kyryllin[52] ,
D. Lacarrere[49] , P. Laguarta Gonzalez[45] , A. Lai[32] , A. Lampis[32] , D. Lancierini[62] ,
C. Landesa Gomez[47] , J.J. Lane[1] , G. Lanfranchi[28] , C. Langenbruch[22] , J. Langer[19] ,
O. Lantwin[44] , T. Latham[57] , F. Lazzari[35,u,49] , C. Lazzeroni[54] , R. Le Gac[13] , H.
Lee[61] , R. Lefèvre[11] , A. Leflat[44] , S. Legotin[44] , M. Lehuraux[57] , E. Lemos Cid[49] ,
O. Leroy[13] , T. Lesiak[41] , E. D. Lesser[49] , B. Leverington[22] , A. Li[4,d] , C. Li[4,d] , C.
Li[13] , H. Li[73] , J. Li[8] , K. Li[76] , L. Li[63] , M. Li[8] , P. Li[7] , P.-R. Li[74] , Q. Li[5,7] ,
T. Li[72] , T. Li[73] , Y. Li[8] , Y. Li[5] , Y. Li[4] , Z. Lian[4,d] , Q. Liang[8] , X. Liang[69] , Z.
Liang[32] , S. Libralon[48] , A. L. Lightbody[12] , C. Lin[7] , T. Lin[58] , R. Lindner[49] , H.
Linton[62] , R. Litvinov[32] , D. Liu[8] , F. L. Liu[1] , G. Liu[73] , K. Liu[74] , S. Liu[5,7] , W.
Liu[8] , Y. Liu[59] , Y. Liu[74] , Y. L. Liu[62] , G. Loachamin Ordonez[70] ,
A. Lobo Salvia[45] , A. Loi[32] , T. Long[56] , F. C. L. Lopes[2,a] , J.H. Lopes[3] ,
A. Lopez Huertas[45] , C. Lopez Iribarnegaray[47] , S. López Soliño[47] , Q. Lu[15] ,
C. Lucarelli[49] , D. Lucchesi[33,r] , M. Lucio Martinez[48] , Y. Luo[6] , A. Lupato[33,j] ,
E. Luppi[26,m] , K. Lynch[23] , X.-R. Lyu[7] , G. M. Ma[4,d] , H. Ma[72] , S. Maccolini[19] ,
F. Machefert[14] , F. Maciuc[43] , B. Mack[69] , I. Mackay[64] , L. M. Mackey[69] ,
L.R. Madhan Mohan[56] , M. J. Madurai[54] , D. Magdalinski[38] , D. Maisuzenko[44] ,
J.J. Malczewski[41] , S. Malde[64] , L. Malentacca[49] , A. Malinin[44] , T. Maltsev[44] ,
G. Manca[32,l] , G. Mancinelli[13] , C. Mancuso[14] , R. Manera Escalero[45] , F. M.
Manganella[37] , D. Manuzzi[25] , D. Marangotto[30,o] , J.F. Marchand[10] ,
R. Marchevski[50] , U. Marconi[25] , E. Mariani[16] , S. Mariani[49] , C. Marin Benito[45] ,
J. Marks[22] , A.M. Marshall[55] , L. Martel[64] , G. Martelli[34] , G. Martellotti[36] ,
L. Martinazzoli[49] , M. Martinelli[31,p] , D. Martinez Gomez[81] , D. Martinez Santos[84] ,
F. Martinez Vidal[48] , A. Martorell i Granollers[46] , A. Massafferri[2] , R. Matev[49] ,
A. Mathad[49] , V. Matiunin[44] , C. Matteuzzi[69] , K.R. Mattioli[15] , A. Mauri[62] ,
E. Maurice[15] , J. Mauricio[45] , P. Mayencourt[50] , J. Mazorra de Cos[48] , M. Mazurek[42] ,
M. McCann[62] , T.H. McGrath[63] , N.T. McHugh[60] , A. McNab[63] , R. McNulty[23] ,
B. Meadows[66] , G. Meier[19] , D. Melnychuk[42] , D. Mendoza Granada[16] , P.
Menendez Valdes Perez[47] , F. M. Meng[4,d] , M. Merk[38,82] , A. Merli[50,30] ,
L. Meyer Garcia[67] , D. Miao[5,7] , H. Miao[7] , M. Mikhasenko[78] , D.A. Milanes[77,z] ,
A. Minotti[31,p] , E. Minucci[28] , T. Miralles[11] , B. Mitreska[19] , D.S. Mitzel[19] , R.
Mocanu[43] , A. Modak[58] , L. Moeser[19] , R.D. Moise[17] , E. F. Molina Cardenas[87] ,
T. Mombächer[49] , M. Monk[57,1] , S. Monteil[11] , A. Morcillo Gomez[47] , G. Morello[28] ,
M.J. Morello[35,t] , M.P. Morgenthaler[22] , A. Moro[31,p] , J. Moron[40] , W. Morren[38] ,
A.B. Morris[49] , A.G. Morris[13] , R. Mountain[69] , H. Mu[4,d] , Z. M. Mu[6] ,
E. Muhammad[57] , F. Muheim[59] , M. Mulder[81] , K. Müller[51] , F. Muñoz-Rojas[9] ,
R. Murta[62] , V. Mytrochenko[52] , P. Naik[61] , T. Nakada[50] , R. Nandakumar[58] ,
T. Nanut[49] , I. Nasteva[3] , M. Needham[59] , E. Nekrasova[44] , N. Neri[30,o] ,

S. Neubert[18], N. Neufeld[49], P. Neustroev[44], J. Nicolini[49], D. Nicotra[82], E.M. Niel[15],
N. Nikitin[44], L. Nisi[19], Q. Niu[74], P. Nogarolli[3], P. Nogga[18], C. Normand[55],
J. Novoa Fernandez[47], G. Nowak[66], C. Nunez[87], H. N. Nur[60],
A. Oblakowska-Mucha[40], V. Obraztsov[44], T. Oeser[17], A. Okhotnikov[44],
O. Okhrimenko[53], R. Oldeman[32,l], F. Oliva[59,49], E. Olivart Pino[45], M. Olocco[19],
C.J.G. Onderwater[82], R.H. O'Neil[49], J.S. Ordonez Soto[11], D. Osthues[19],
J.M. Otalora Goicochea[3], P. Owen[51], A. Oyanguren[48], O. Ozcelik[49], F. Paciolla[35,x],
A. Padee[42], K.O. Padeken[18], B. Pagare[47], T. Pajero[49], A. Palano[24],
M. Palutan[28], C. Pan[75], X. Pan[4,d], S. Panebianco[12], G. Panshin[5],
L. Paolucci[63], A. Papanestis[58], M. Pappagallo[24,i], L.L. Pappalardo[26],
C. Pappenheimer[66], C. Parkes[63], D. Parmar[78], B. Passalacqua[26,m], G. Passaleva[27],
D. Passaro[35,t,49], A. Pastore[24], M. Patel[62], J. Patoc[64], C. Patrignani[25,k], A.
Paul[69], C.J. Pawley[82], A. Pellegrino[38], J. Peng[5,7], X. Peng[74], M. Pepe Altarelli[28],
S. Perazzini[25], D. Pereima[44], H. Pereira Da Costa[68], M. Pereira Martinez[47],
A. Pereiro Castro[47], C. Perez[46], P. Perret[11], A. Perrevoort[81], A. Perro[49,13],
M.J. Peters[66], K. Petridis[55], A. Petrolini[29,n], S. Pezzulo[29,n], J. P. Pfaller[66],
H. Pham[69], L. Pica[35,t], M. Piccini[34], L. Piccolo[32], B. Pietrzyk[10], G. Pietrzyk[14],
R. N. Pilato[61], D. Pinci[36], F. Pisani[49], M. Pizzichemi[31,p,49], V. M. Placinta[43],
M. Plo Casasus[47], T. Poeschl[49], F. Polci[16], M. Poli Lener[28], A. Poluektov[13],
N. Polukhina[44], I. Polyakov[63], E. Polycarpo[3], S. Ponce[49], D. Popov[7,49],
S. Poslavskii[44], K. Prasanth[59], C. Prouve[84], D. Provenzano[32,l,49], V. Pugatch[53],
G. Punzi[35,u], J.R. Pybus[68], S. Qasim[51], Q. Q. Qian[6], W. Qian[7], N. Qin[4,d],
S. Qu[4,d], R. Quagliani[49], R.I. Rabadan Trejo[57], R. Racz[80], J.H. Rademacker[55],
M. Rama[35], M. Ramírez García[87], V. Ramos De Oliveira[70], M. Ramos Pernas[57],
M.S. Rangel[3], F. Ratnikov[44], G. Raven[39], M. Rebollo De Miguel[48], F. Redi[30,j],
J. Reich[55], F. Reiss[20], Z. Ren[7], P.K. Resmi[64], M. Ribalda Galvez[45],
R. Ribatti[50], G. Ricart[15,12], D. Riccardi[35,t], S. Ricciardi[58], K. Richardson[65],
M. Richardson-Slipper[56], K. Rinnert[61], P. Robbe[14,49], G. Robertson[60],
E. Rodrigues[61], A. Rodriguez Alvarez[45], E. Rodriguez Fernandez[47],
J.A. Rodriguez Lopez[77], E. Rodriguez Rodriguez[49], J. Roensch[19], A. Rogachev[44],
A. Rogovskiy[58], D.L. Rolf[19], P. Roloff[49], V. Romanovskiy[66], A. Romero Vidal[47],
G. Romolini[26,49], F. Ronchetti[50], T. Rong[6], M. Rotondo[28], S. R. Roy[22],
M.S. Rudolph[69], M. Ruiz Diaz[22], R.A. Ruiz Fernandez[47], J. Ruiz Vidal[82], J.
J. Saavedra-Arias[9], J.J. Saborido Silva[47], S. E. R. Sacha Emile R.[49], N. Sagidova[44],
D. Sahoo[79], N. Sahoo[54], B. Saitta[32,l], M. Salomoni[31,49,p], I. Sanderswood[48],
R. Santacesaria[36], C. Santamarina Rios[47], M. Santimaria[28], L. Santoro [2],
E. Santovetti[37], A. Saputi[26,49], D. Saranin[44], A. Sarnatskiy[81], G. Sarpis[49],
M. Sarpis[80], C. Satriano[36,v], A. Satta[37], M. Saur[74], D. Savrina[44], H. Sazak[17],
F. Sborzacchi[49,28], A. Scarabotto[19], S. Schael[17], S. Scherl[61], M. Schiller[22],
H. Schindler[49], M. Schmelling[21], B. Schmidt[49], N. Schmidt[68], S. Schmitt[65],
H. Schmitz[18], O. Schneider[50], A. Schopper[62], N. Schulte[19], M.H. Schune[14],
G. Schwering[17], B. Sciascia[28], A. Sciuccati[49], G. Scriven[82], I. Segal[78],
S. Sellam[47], A. Semennikov[44], T. Senger[51], M. Senghi Soares[39], A. Sergi[29,n,49],
N. Serra[51], L. Sestini[27], A. Seuthe[19], B. Sevilla Sanjuan[46], Y. Shang[6],
D.M. Shangase[87], M. Shapkin[44], R. S. Sharma[69], I. Shchemerov[44], L. Shchutska[50],
T. Shears[61], L. Shekhtman[44], Z. Shen[38], S. Sheng[5,7], V. Shevchenko[44], B. Shi[7],
Q. Shi[7], W. S. Shi[73], Y. Shimizu[14], E. Shmanin[25], R. Shorkin[44],
J.D. Shupperd[69], R. Silva Coutinho[2], G. Simi[33,r], S. Simone[24,i], M. Singha[79],
N. Skidmore[57], T. Skwarnicki[69], M.W. Slater[54], E. Smith[65], K. Smith[68],
M. Smith[62], L. Soares Lavra[59], M.D. Sokoloff[66], F.J.P. Soler[60], A. Solomin[55],

31

A. Solovev[44] , K. Solovieva[20] , N. S. Sommerfeld[18] , R. Song[1] , Y. Song[50] ,
Y. Song[4,d] , Y. S. Song[6] , F.L. Souza De Almeida[69] , B. Souza De Paula[3] ,
K.M. Sowa[40] , E. Spadaro Norella[29,n] , E. Spedicato[25] , J.G. Speer[19] , P. Spradlin[60] ,
V. Sriskaran[49] , F. Stagni[49] , M. Stahl[78] , S. Stahl[49] , S. Stanislaus[64] , M.
Stefaniak[88] , E.N. Stein[49] , O. Steinkamp[51] , H. Stevens[19] , D. Strekalina[44] , Y. Su[7] ,
F. Suljik[64] , J. Sun[32] , J. Sun[63] , L. Sun[75] , D. Sundfeld[2] , W. Sutcliffe[51] ,
V. Svintozelskyi[48] , K. Swientek[40] , F. Swystun[56] , A. Szabelski[42] , T. Szumlak[40] ,
Y. Tan[4,d] , Y. Tang[75] , Y. T. Tang[7] , M.D. Tat[22] , J. A. Teijeiro Jimenez[47] ,
A. Terentev[44] , F. Terzuoli[35,x] , F. Teubert[49] , E. Thomas[49] , D.J.D. Thompson[54] , A.
R. Thomson-Strong[59] , H. Tilquin[62] , V. Tisserand[11] , S. T'Jampens[10] , M. Tobin[5,49] ,
T. T. Todorov[20] , L. Tomassetti[26,m] , G. Tonani[30] , X. Tong[6] , T. Tork[30] ,
D. Torres Machado[2] , L. Toscano[19] , D.Y. Tou[4,d] , C. Trippl[46] , G. Tuci[22] ,
N. Tuning[38] , L.H. Uecker[22] , A. Ukleja[40] , D.J. Unverzagt[22] , A. Upadhyay[49] , B.
Urbach[59] , A. Usachov[39] , A. Ustyuzhanin[44] , U. Uwer[22] , V. Vagnoni[25,49] , V.
Valcarce Cadenas[47] , G. Valenti[25] , N. Valls Canudas[49] , J. van Eldik[49] ,
H. Van Hecke[68] , E. van Herwijnen[62] , C.B. Van Hulse[47,aa] , R. Van Laak[50] ,
M. van Veghel[38] , G. Vasquez[51] , R. Vazquez Gomez[45] , P. Vazquez Regueiro[47] ,
C. Vázquez Sierra[84] , S. Vecchi[26] , J. Velilla Serna[48] , J.J. Velthuis[55] , M. Veltri[27,y] ,
A. Venkateswaran[50] , M. Verdoglia[32] , M. Vesterinen[57] , W. Vetens[69] , D.
Vico Benet[64] , P. Vidrier Villalba[45] , M. Vieites Diaz[47,49] , X. Vilasis-Cardona[46] ,
E. Vilella Figueras[61] , A. Villa[25] , P. Vincent[16] , B. Vivacqua[3] , F.C. Volle[54] ,
D. vom Bruch[13] , N. Voropaev[44] , K. Vos[82] , C. Vrahas[59] , J. Wagner[19] , J. Walsh[35] ,
E.J. Walton[1,57] , G. Wan[6] , A. Wang[7] , B. Wang[5] , C. Wang[22] , G. Wang[8] ,
H. Wang[74] , J. Wang[6] , J. Wang[5] , J. Wang[4,d] , J. Wang[75] , M. Wang[49] , N. W.
Wang[7] , R. Wang[55] , X. Wang[8] , X. Wang[73] , X. W. Wang[62] , Y. Wang[76] ,
Y. Wang[6] , Y. H. Wang[74] , Z. Wang[14] , Z. Wang[30] , J.A. Ward[57] , M. Waterlaat[49] ,
N.K. Watson[54] , D. Websdale[62] , Y. Wei[6] , Z. Weida[7] , J. Wendel[84] ,
B.D.C. Westhenry[55] , C. White[56] , M. Whitehead[60] , E. Whiter[54] ,
A.R. Wiederhold[63] , D. Wiedner[19] , M. A. Wiegertjes[38] , C. Wild[64] ,
G. Wilkinson[64,49] , M.K. Wilkinson[66] , M. Williams[65] , M. J. Williams[49] ,
M.R.J. Williams[59] , R. Williams[56] , S. Williams[55] , Z. Williams[55] , F.F. Wilson[58] ,
M. Winn[12] , W. Wislicki[42] , M. Witek[41] , L. Witola[19] , T. Wolf[22] , E. Wood[56] ,
G. Wormser[14] , S.A. Wotton[56] , H. Wu[69] , J. Wu[8] , X. Wu[75] , Y. Wu[6,56] , Z. Wu[7] ,
K. Wyllie[49] , S. Xian[73] , Z. Xiang[5] , Y. Xie[8] , T. X. Xing[30] , A. Xu[35,t] , L. Xu[4,d] ,
L. Xu[4,d] , M. Xu[49] , Z. Xu[49] , Z. Xu[7] , Z. Xu[5] , K. Yang[62] , X. Yang[6] ,
Y. Yang[15] , Z. Yang[6] , V. Yeroshenko[14] , H. Yeung[63] , H. Yin[8] , X. Yin[7] , C. Y.
Yu[6] , J. Yu[72] , X. Yuan[5] , Y Yuan[5,7] , E. Zaffaroni[50] , J. A. Zamora Saa[71] ,
M. Zavertyaev[21] , M. Zdybal[41] , F. Zenesini[25] , C. Zeng[5,7] , M. Zeng[4,d] , C. Zhang[6] ,
D. Zhang[8] , J. Zhang[7] , L. Zhang[4,d] , R. Zhang[8] , S. Zhang[72] , S. Zhang[64] ,
Y. Zhang[6] , Y. Z. Zhang[4,d] , Z. Zhang[4,d] , Y. Zhao[22] , A. Zhelezov[22] , S. Z. Zheng[6] ,
X. Z. Zheng[4,d] , Y. Zheng[7] , T. Zhou[6] , X. Zhou[8] , Y. Zhou[7] , V. Zhovkovska[57] , L.
Z. Zhu[7] , X. Zhu[4,d] , X. Zhu[8] , Y. Zhu[17] , V. Zhukov[17] , J. Zhuo[48] , Q. Zou[5,7] ,
D. Zuliani[33,r] , G. Zunica[28] .

[1] School of Physics and Astronomy, Monash University, Melbourne, Australia
[2] Centro Brasileiro de Pesquisas Físicas (CBPF), Rio de Janeiro, Brazil
[3] Universidade Federal do Rio de Janeiro (UFRJ), Rio de Janeiro, Brazil
[4] Department of Engineering Physics, Tsinghua University, Beijing, China
[5] Institute Of High Energy Physics (IHEP), Beijing, China
[6] School of Physics State Key Laboratory of Nuclear Physics and Technology, Peking University, Beijing, China

[7]University of Chinese Academy of Sciences, Beijing, China

[8]Institute of Particle Physics, Central China Normal University, Wuhan, Hubei, China

[9]Consejo Nacional de Rectores (CONARE), San Jose, Costa Rica

[10]Université Savoie Mont Blanc, CNRS, IN2P3-LAPP, Annecy, France

[11]Université Clermont Auvergne, CNRS/IN2P3, LPC, Clermont-Ferrand, France

[12]Université Paris-Saclay, Centre d'Etudes de Saclay (CEA), IRFU, Saclay, France, Gif-Sur-Yvette, France

[13]Aix Marseille Univ, CNRS/IN2P3, CPPM, Marseille, France

[14]Université Paris-Saclay, CNRS/IN2P3, IJCLab, Orsay, France

[15]Laboratoire Leprince-Ringuet, CNRS/IN2P3, Ecole Polytechnique, Institut Polytechnique de Paris, Palaiseau, France

[16]LPNHE, Sorbonne Université, Paris Diderot Sorbonne Paris Cité, CNRS/IN2P3, Paris, France

[17]I. Physikalisches Institut, RWTH Aachen University, Aachen, Germany

[18]Universität Bonn - Helmholtz-Institut für Strahlen und Kernphysik, Bonn, Germany

[19]Fakultät Physik, Technische Universität Dortmund, Dortmund, Germany

[20]Physikalisches Institut, Albert-Ludwigs-Universität Freiburg, Freiburg, Germany

[21]Max-Planck-Institut für Kernphysik (MPIK), Heidelberg, Germany

[22]Physikalisches Institut, Ruprecht-Karls-Universität Heidelberg, Heidelberg, Germany

[23]School of Physics, University College Dublin, Dublin, Ireland

[24]INFN Sezione di Bari, Bari, Italy

[25]INFN Sezione di Bologna, Bologna, Italy

[26]INFN Sezione di Ferrara, Ferrara, Italy

[27]INFN Sezione di Firenze, Firenze, Italy

[28]INFN Laboratori Nazionali di Frascati, Frascati, Italy

[29]INFN Sezione di Genova, Genova, Italy

[30]INFN Sezione di Milano, Milano, Italy

[31]INFN Sezione di Milano-Bicocca, Milano, Italy

[32]INFN Sezione di Cagliari, Monserrato, Italy

[33]INFN Sezione di Padova, Padova, Italy

[34]INFN Sezione di Perugia, Perugia, Italy

[35]INFN Sezione di Pisa, Pisa, Italy

[36]INFN Sezione di Roma La Sapienza, Roma, Italy

[37]INFN Sezione di Roma Tor Vergata, Roma, Italy

[38]Nikhef National Institute for Subatomic Physics, Amsterdam, Netherlands

[39]Nikhef National Institute for Subatomic Physics and VU University Amsterdam, Amsterdam, Netherlands

[40]AGH - University of Krakow, Faculty of Physics and Applied Computer Science, Kraków, Poland

[41]Henryk Niewodniczanski Institute of Nuclear Physics Polish Academy of Sciences, Kraków, Poland

[42]National Center for Nuclear Research (NCBJ), Warsaw, Poland

[43]Horia Hulubei National Institute of Physics and Nuclear Engineering, Bucharest-Magurele, Romania

[44]Authors affiliated with an institute formerly covered by a cooperation agreement with CERN.

[45]ICCUB, Universitat de Barcelona, Barcelona, Spain

[46]La Salle, Universitat Ramon Llull, Barcelona, Spain

[47]Instituto Galego de Física de Altas Enerxías (IGFAE), Universidade de Santiago de Compostela, Santiago de Compostela, Spain

[48]Instituto de Fisica Corpuscular, Centro Mixto Universidad de Valencia - CSIC, Valencia, Spain

[49]European Organization for Nuclear Research (CERN), Geneva, Switzerland

[50]Institute of Physics, Ecole Polytechnique Fédérale de Lausanne (EPFL), Lausanne, Switzerland

[51]Physik-Institut, Universität Zürich, Zürich, Switzerland

[52]NSC Kharkiv Institute of Physics and Technology (NSC KIPT), Kharkiv, Ukraine

[53]Institute for Nuclear Research of the National Academy of Sciences (KINR), Kyiv, Ukraine

[54]School of Physics and Astronomy, University of Birmingham, Birmingham, United Kingdom

[55]H.H. Wills Physics Laboratory, University of Bristol, Bristol, United Kingdom

[56]Cavendish Laboratory, University of Cambridge, Cambridge, United Kingdom

[57]Department of Physics, University of Warwick, Coventry, United Kingdom

[58]STFC Rutherford Appleton Laboratory, Didcot, United Kingdom

[59] School of Physics and Astronomy, University of Edinburgh, Edinburgh, United Kingdom

[60] School of Physics and Astronomy, University of Glasgow, Glasgow, United Kingdom

[61] Oliver Lodge Laboratory, University of Liverpool, Liverpool, United Kingdom

[62] Imperial College London, London, United Kingdom

[63] Department of Physics and Astronomy, University of Manchester, Manchester, United Kingdom

[64] Department of Physics, University of Oxford, Oxford, United Kingdom

[65] Massachusetts Institute of Technology, Cambridge, MA, United States

[66] University of Cincinnati, Cincinnati, OH, United States

[67] University of Maryland, College Park, MD, United States

[68] Los Alamos National Laboratory (LANL), Los Alamos, NM, United States

[69] Syracuse University, Syracuse, NY, United States

[70] Pontifícia Universidade Católica do Rio de Janeiro (PUC-Rio), Rio de Janeiro, Brazil, associated to [3]

[71] Universidad Andres Bello, Santiago, Chile, associated to [51]

[72] School of Physics and Electronics, Hunan University, Changsha City, China, associated to [8]

[73] Guangdong Provincial Key Laboratory of Nuclear Science, Guangdong-Hong Kong Joint Laboratory of Quantum Matter, Institute of Quantum Matter, South China Normal University, Guangzhou, China, associated to [4]

[74] Lanzhou University, Lanzhou, China, associated to [5]

[75] School of Physics and Technology, Wuhan University, Wuhan, China, associated to [4]

[76] Henan Normal University, Xinxiang, China, associated to [8]

[77] Departamento de Fisica , Universidad Nacional de Colombia, Bogota, Colombia, associated to [16]

[78] Ruhr Universitaet Bochum, Fakultaet f. Physik und Astronomie, Bochum, Germany, associated to [19]

[79] Eotvos Lorand University, Budapest, Hungary, associated to [49]

[80] Faculty of Physics, Vilnius University, Vilnius, Lithuania, associated to [20]

[81] Van Swinderen Institute, University of Groningen, Groningen, Netherlands, associated to [38]

[82] Universiteit Maastricht, Maastricht, Netherlands, associated to [38]

[83] Tadeusz Kosciuszko Cracow University of Technology, Cracow, Poland, associated to [41]

[84] Universidade da Coruña, A Coruña, Spain, associated to [46]

[85] Department of Physics and Astronomy, Uppsala University, Uppsala, Sweden, associated to [60]

[86] Taras Schevchenko University of Kyiv, Faculty of Physics, Kyiv, Ukraine, associated to [14]

[87] University of Michigan, Ann Arbor, MI, United States, associated to [69]

[88] Ohio State University, Columbus, United States, associated to [68]

[a] Universidade Estadual de Campinas (UNICAMP), Campinas, Brazil

[b] Centro Federal de Educacão Tecnológica Celso Suckow da Fonseca, Rio De Janeiro, Brazil

[c] Department of Physics and Astronomy, University of Victoria, Victoria, Canada

[d] Center for High Energy Physics, Tsinghua University, Beijing, China

[e] Hangzhou Institute for Advanced Study, UCAS, Hangzhou, China

[f] LIP6, Sorbonne Université, Paris, France

[g] Lamarr Institute for Machine Learning and Artificial Intelligence, Dortmund, Germany

[h] Universidad Nacional Autónoma de Honduras, Tegucigalpa, Honduras

[i] Università di Bari, Bari, Italy

[j] Università di Bergamo, Bergamo, Italy

[k] Università di Bologna, Bologna, Italy

[l] Università di Cagliari, Cagliari, Italy

[m] Università di Ferrara, Ferrara, Italy

[n] Università di Genova, Genova, Italy

[o] Università degli Studi di Milano, Milano, Italy

[p] Università degli Studi di Milano-Bicocca, Milano, Italy

[q] Università di Modena e Reggio Emilia, Modena, Italy

[r] Università di Padova, Padova, Italy

[s] Università di Perugia, Perugia, Italy

[t] Scuola Normale Superiore, Pisa, Italy

[u] Università di Pisa, Pisa, Italy

[v] Università della Basilicata, Potenza, Italy

[w] Università di Roma Tor Vergata, Roma, Italy

[x] Università di Siena, Siena, Italy

[y] *Università di Urbino, Urbino, Italy*
[z] *Universidad de Ingeniería y Tecnología (UTEC), Lima, Peru*
[aa] *Universidad de Alcalá, Alcalá de Henares , Spain*

[†] *Deceased*